



Cite this: *Mater. Horiz.*, 2024, 11, 5914

## Anode-free post-Li metal batteries

Deik Petersen,<sup>a</sup> Monja Gronenberg,<sup>a</sup> German Lener,<sup>b</sup> Ezequiel P. M. Leiva,<sup>b</sup> Guillermina L. Luque,<sup>\*b</sup> Sasan Rostami,<sup>c</sup> Andrea Paoletta,<sup>d</sup> Bing Joe Hwang,<sup>e</sup> Rainer Adelung  <sup>a</sup> and Mozaffar Abdollahifar  <sup>\*a</sup><sup>e</sup>

Anode-free metal batteries (AFMBs) are a new architecture of battery technology that relies solely on current collectors (CCs) at the anode side, eliminating the need for traditional metal anodes. This approach can pave the way for higher energy densities, lower manufacturing costs, and lower environmental footprints associated with metal batteries. This comprehensive review provides an in-depth exploration of AFMB technology, extending its scope beyond lithium and into a broader range of metals (sodium Na, potassium K, magnesium Mg, zinc Zn and aluminum Al). The concept of "metal-philicity" is discussed, which plays a pivotal role in understanding and controlling metal plating behavior within AFMBs, and also computational studies that employ first-principles calculations. This novel notion offers valuable insights into the interactions between metals and CC surfaces, which are essential for designing efficient battery systems. Moreover, the review explores various materials and experimental methods to enhance metal plating efficiency while mitigating issues such as dendrite formation through the realm of surface modifications and coatings on CCs. By providing a deeper understanding of strategies for optimizing anode-free post-Li metal battery technologies, this review aims to contribute to developing more efficient, sustainable, and cost-effective energy storage for the near future.

Received 3rd May 2024,  
Accepted 6th September 2024

DOI: 10.1039/d4mh00529e

[rsc.li/materials-horizons](http://rsc.li/materials-horizons)

### Wider impact

The global demand for more efficient and sustainable energy storage solutions has increased significantly in recent years. Traditional battery technologies face limitations regarding energy density, manufacturing costs, and environmental impact. In response, researchers and industries have been exploring new materials and architectures to overcome these challenges. Anode-free metal batteries (AFMBs) have emerged as a promising solution that can eliminate the need for traditional metal anodes, relying solely on current collectors (CCs) placed at the anode side and use of a cathode as the sole active material, paving the way for higher energy densities and potentially lower manufacturing costs and environmental footprints associated with metal batteries. Therefore, innovative solutions for CC chemistries *via* surface modifications and coatings while mitigating issues such as dendrite formation are aimed at optimizing AFMBs. Central to the discussion is the "metal-philicity" concept, which plays a pivotal role in understanding and controlling metal-plating behavior within AFMBs beyond lithium metal batteries. Through computational studies employing first-principles calculations, researchers gain valuable insights into the interactions between metals and CC surfaces, essential for designing efficient battery systems. Ultimately, this review serves as a guiding beacon for researchers, offering a deeper understanding of the strategies necessary to optimize the CC of AFMBs.

<sup>a</sup> Chair for Functional Nanomaterials, Department of Materials Science, Faculty of Engineering, Kiel University, Kaiserstr. 2, 24143, Kiel, Germany.

E-mail: [moza@tf.uni-kiel.de](mailto:moza@tf.uni-kiel.de)

<sup>b</sup> Departamento de Química Teórica y Computacional, INFIQC, Av Medina Allende y Haya de la Torre, Ciudad Universitaria, CP X5000HUA Córdoba, Argentina.

E-mail: [guillerminaluque@unc.edu.ar](mailto:guillerminaluque@unc.edu.ar)

<sup>c</sup> Department of Physics and Energy Engineering, Amirkabir University of Technology (Tehran Polytechnique), Tehran, Iran

<sup>d</sup> Dipartimento di Scienze Chimiche e Geologiche e Università degli Studi di Modena e Reggio Emilia Via Campi 103, Modena 41125, Italy

<sup>e</sup> Sustainable Electrochemical Energy Development Center, National Taiwan University of Science and Technology, Taipei 10617, Taiwan



Sasan Rostami

Sasan Rostami received his Bachelor's degree in Physics from Razi University in 2017 and his Master's degree in Condensed Matter Physics from Amirkabir University of Technology in 2020. His master's thesis focused on fabricating electrodes based on two-dimensional materials for lithium-ion batteries and recently he started to work on anode-free concept for sodium-ion and solid-state batteries.

## 1. Introduction

As global energy demands will likely continue to rise for the foreseeable future, the pressing challenge of energy storage capacity emerges as a critical bottleneck.<sup>1–3</sup> While renewable sources like solar and wind power offer sustainable alternatives to fossil fuels, their intermittent nature intensifies the need for reliable and scalable storage solutions on various timescales.<sup>4</sup> The limitation in storage technology due to various restrictions like a high price and short life cycle impedes the integration of renewable energy into existing grids, underscoring the importance of finding accessible, low-cost, and stable energy storage systems. In this context, batteries play a key role as they efficiently cover the role of mid-term (hours-weeks) storage

and offer high energy densities, scalability, and an exceptional power efficiency approaching 100%.<sup>5</sup> Comparing batteries to large energy storage systems like hydroelectric power stations, which currently contribute to over 90% of the worldwide storage capacity, battery storage offers the potential for decentralization and does not have geological requirements. The state-of-the-art batteries almost exclusively use lithium (Li) ions as the mobile charge carrier due to Li having the lowest electrochemical potential and therefore the highest power density per charge. Li-ion batteries (LIBs) are widely used in the transportation sector and are the preferred energy storage system for portable electronic devices.<sup>6</sup> However, Li is not an abundant metal in the earth's crust, and currently rare elements like nickel (Ni) and cobalt (Co) are used for the cathode.



**From left to right:** Deik Petersen, Monja Gronenberg, Rainer Adelung and Mozaffar Abdollahifar

*Mozaffar Abdollahifar received his doctorate focused on energy storage materials from the National Taiwan University (NTU). Before becoming a battery group leader at Kiel University, he worked as a scientist for several years at NTU and then at the Battery LabFactory Braunschweig (BLB). He is interested in developing supercapacitors and battery materials for Li, Na and sulfur chemistries, electrode design and production, as well as recycling end-of-life batteries.*



**From left to right:** German Lener, Guillermina L. Luque and Ezequiel P. M. Leiva

*at the Department of Theoretical and Computational Chemistry, Faculty of Chemical Sciences, UNC, CONICET. He has made significant contributions to lithium-ion battery research and theoretical electrochemistry, having published over 200 articles and holding one patent. His work includes pioneering projects, such as leading the installation of Argentina's fastest supercomputer for nanoscience simulations.*



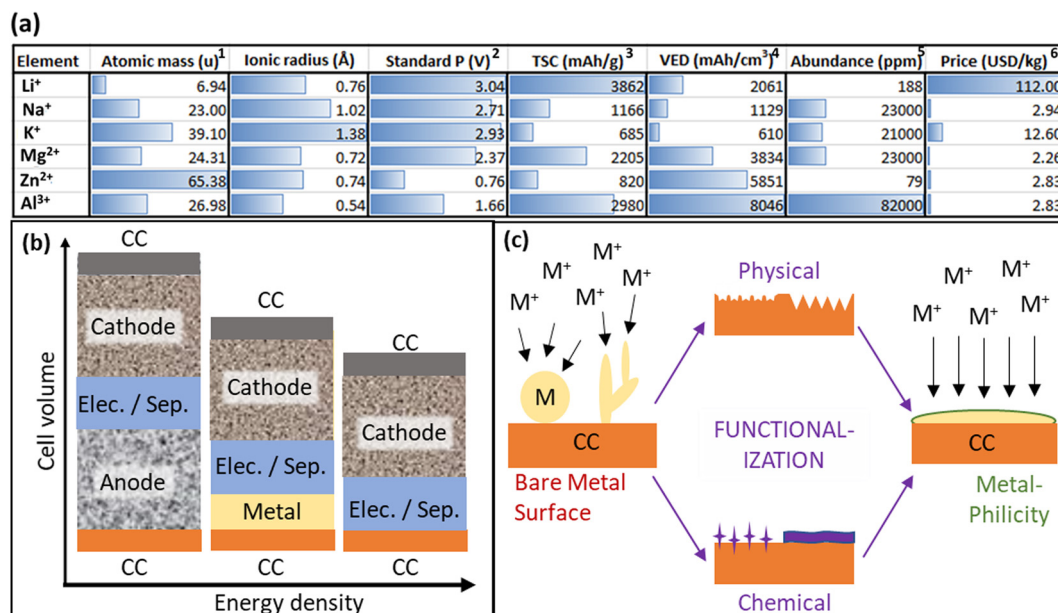


Fig. 1 (a) A compression of post-Li-ions ( $\text{Li}^+$ ,  $\text{Na}^+$ ,  $\text{K}^+$ ,  $\text{Mg}^{2+}$ ,  $\text{Zn}^{2+}$ ,  $\text{Al}^{3+}$ ): (1) relative atomic mass, (2) standard potential (V) vs. standard hydrogen electrode (SHE), and the values are negative. (3) theoretical specific capacity, (4) volumetric energy density, (5) crustal abundance, (6) data costs obtained from.<sup>8</sup> (b) Schematic illustration of cell volume for (left) a conventional metal-ion battery with an anode, (middle) a metal battery (MB) with a metallic anode like Li, Na, K, etc., often denoted as 'half-cell' for cathode testing, and (right) an anode-free metal battery (AFMB) using just a current collector (CC) as a nucleation site for the metal anode. The cathode is fixed, and the electrolyte could be a solid electrolyte or a liquid electrolyte with a separator. The AFMB clearly enables the highest volumetric energy density compared to a conventional metal-ion battery and a MB. (c) Schematic representation of how a functionalization of the metal-CC-interface can guide the metal growth from a dendritic and non-uniform plating to a planar growth by changing the surface energy of the CC.

This is especially relevant in geopolitical terms, since most of the supply is concentrated only in a few countries. This leads to a risk of supply instability and the possibility of price increments, which poses a high risk when implementing an energy infrastructure strongly reliant on storage capacity. Furthermore, the price of Li and the components of the electrolyte are expensive compared to other possible metals like sodium (Na) or aluminum (Al) (Fig. 1a). In this context, the approach of metal anodes has recently gained a lot of scientific attention. In a historical context, this principle is not a new approach, the first LIB ever built by M. Stanley Whittingham in the 1970s used Li-metal as the anode material, however, their commercialization failed because of the high safety risks of dendrite formation which caused the ignition of the batteries, as well as the discovery of an intercalation type anode by Akira Yoshino in 1983. Since then, carbon-based approaches for the anode material have dominated in the scientific community<sup>7</sup> but the demand for higher power densities and faster charging time rose sharply due to the successful introduction of electric vehicles.

Anode-free metal batteries (AFMBs) represent a groundbreaking approach to energy storage by eliminating the conventional anode component found in metal batteries (MBs). Having a look at Fig. 1b, it becomes clear that AFMBs have the perspective of achieving significantly higher energy densities compared to traditional metal-ion batteries. This increased energy density can translate to longer-lasting and more

powerful energy storage solutions for applications ranging from consumer electronics to electric vehicles. In addition, eliminating the anode simplifies the battery structure, potentially reducing manufacturing costs and making these batteries more economically viable on a larger scale. By reducing the components needed for battery assembly, not only the costs but also the energy consumption during manufacturing can eventually be decreased, resulting in a reduced environmental impact.

## 2. Fundamentals of anode-free metal batteries

The terms anode-free and anode-less are used interchangeably in the context of metal battery technology. Both are used as buzzwords to describe a battery design that lacks a traditional anode material and do not describe actual physics. The anode is *in situ* formed by electroplating metal ions on the anodic current collector (CC) during the charging process and is stripped during the discharge. In this review, "anode-free" will be used since this terminology seems to prevail over "anode-less".<sup>9</sup> In AFMBs, a cathode and the electrolyte are the only sources of metal-ions. During the charging of an AFMB, metal-ions are released from the cathode material and plated on the current collector (CC) on the other side of the separator. From this point on, an AFMB (Fig. 1b) basically faces the same



challenges as any MB, which is mainly the risk of dendrite formation upon repetitive plating/stripping of the metal<sup>10–13</sup> (in some studies “deposition”<sup>14,15</sup> was used, however, in this manuscript “plating” is fixed), as well as the decrease of capacity by the loss of metal-ions through the formation of ‘dead metal’ or components of the solid electrolyte interface (SEI). Another challenge that AFMBs as well as MBs face is the volume change during the metal plating/stripping. AFMBs and MBs also share the same safety concerns, *i.e.* if the battery pack is damaged and the alkali metal is exposed to water or humid air, it will catch fire and react violently. As can be seen in Fig. 1a, by changing the metal-ion, some post-Li metal batteries (PLMBs) could potentially outperform LIBs for certain applications like stationary and large-scale storage systems. Metal-ions such as Mg<sup>2+</sup> or Al<sup>3+</sup> that carry more than one charge per ion can reach higher volumetric energy densities than Li. Batteries with larger alkali metals such as Na- and K-metal batteries provide a much lower gravimetric and volumetric capacity compared to Li-metal batteries (LMBs). But compared to conventional LIBs with graphite as an anode, all PLMBs can achieve superior energy densities. In addition, they are much more abundant than Li and hence cheaper and can compete with LIBs in various fields of application, such as stationary energy storage systems.<sup>16–20</sup>

Ongoing research and development efforts are actively addressing these hurdles, paving the way for the widespread adoption of this transformative technology in the near future.<sup>17</sup> The main challenge is to enable a homogeneous plating/stripping behavior over hundreds of cycles. Therefore, a homogeneous nucleation of the metal layer during the first cycle is decisive. If the first metal layer that forms on the CC is not flat and homogeneous, the same holds for the SEI that will form and consequently, the local current density will change due to locally enhanced electric field strengths and enhanced transport kinetics. Over the course of several cycles, this can lead to an amplification of the surface roughness and the formation of dead metal or hazardous dendrites, decreasing the structural integrity of the cell.

To ensure homogeneous metal plating conditions – especially during the first cycle – several measures can be taken. For the homogenous nucleation of the metal on the CC, the so-called “metal-philicity” plays a decisive role, *i.e.* the surface of the CC should be functionalized in a way that the metal atoms will preferably bond to the CC surface rather than to form metal–metal bonds. The homogeneity of the metal layer is decisive in enabling a homogeneous current density distribution and long-term cycling stability. The metal-philicity as an important concept that will be explained in more detail in the next section. Another way to homogenize the plating process and to prevent dendrite formation is to introduce a mechanically stable and ionically conductive SEI that cannot be pierced easily by growing dendrites and that ensures the growth of an equally smooth metal surface.

In this review paper, the advances in AFMB technology, particularly on optimizing CCs for a variety of metals such as Na, potassium (K), magnesium (Mg), zinc (Zn), and Al other

than Li, or PLMBs, will be presented and discussed. Fig. 1c gives an overview of the main strategies to increase the number of nucleation sites on the CC that can help to increase the philicity towards the metal to be deposited.<sup>21,22</sup> Generally speaking, the surface can be functionalized by a physical treatment changing the topology and the surface area of the interface or by a chemical treatment changing the surface energy and hence the binding energy towards the metal to be deposited (or by a combination of both). Following the introduction of metal-philicity, computational studies of AFMBs are reviewed and discussed, and challenges and solutions of CC chemistries for each metal in anode-free PLMBs are then addressed in separate sections.

### 3. “Metal-philicity” concept

The term “metal-philicity” (M-philicity, where M can be either Li, Na, K, Mg, Zn, or Al) is the affinity or attraction of a material to metal-ions, considering how good a material can accommodate and interact with the metal-ion during the electrochemical plating/stripping processes. The surface energy, its adsorption ability for the metal, plays a key role in the electric field distribution that takes place on the surface and the electrolyte that circumvents it, also changing the constitution of the SEI layer, contributing finally to the electrochemical performance.<sup>23–25</sup> This is a common property that should be considered independently for any studied AFMB. As considered by Pande *et al.*,<sup>26</sup> as a general term, a good CC material for AFMBs should have a high electronic conductivity, be stable against corrosion, and enable a homogenous metal nucleation leading to a 2D growth and a fast surface diffusion of the metal atoms on the CC surface. By controlling the “M-philicity” of the host material (*e.g.* CC), the plating behavior of the metal during battery charging can be controlled to achieve a stable AFMB with higher energy density, efficiency, and longer cycle life.

For anode-free Li-metal batteries (AFLMB), talking about the lithiophilicity factor, and similarly in the case of anode-free Na-, K-, Mg-, Zn-, and Al-metal batteries, it would be sodiophilicity (for AFSMB), potassiophilicity (for AFKMB), magnesiophilicity (for AFMMB), zincophilicity (for AFZMB), and aluminophilicity (for AFAMB). In each case, a material’s innate attraction and interaction to M-ions or M-metal is referred, significantly impacting the efficiency of M-based battery technologies. Materials demonstrating elevated “metal-philicity” are highly sought after for AFMBs, as they play a critical role in accelerating the plating/stripping of M-ions during (dis)charging processes. This property is vital for maintaining the stability and effectiveness of the AFMB playing an important role to ensure a controlled and uniform growth of reduced metal. For each of the metals, three main steps need to be considered in the nucleation and growth of the metal on the CC to achieve a high-performance AFMB, as discussed for Li-metal by Wang *et al.*<sup>27</sup> The discussion is for AFLMBs, but could be considered for the other metals as well. Firstly, the M-ions have to migrate to the

CC surface under the driving forces of gradient concentration and the electric field force within the battery. Secondly, M-ions near the CC surface electrically contact the surface and reduce to the metallic form, driven by the electrostatic interaction of the nucleation sites and the ions. Finally, the M atoms diffuse over the surface and nucleate. The metal plating is a competitive process of M-M bonding and M-CC bonding. Nevertheless, there is no singular formula to calculate the metal-philicity, since it is related to different parameters such as the binding energy of the M atoms, the nucleation overpotential, the wettability, the electric field and the morphology of the deposited surface as will be further discussed. This clearly goes beyond a purely chemical picture and must also take into account aspects of solid-state physics and crystallography, emphasizing the importance of interdisciplinary research on that topic.

## 4. Computational studies of AFMBs

Theoretical computational studies play an important role in accelerating the discovery of new materials that can be used for providing valuable insights and knowledge about the structures, thermodynamics, diffusion kinetics, and phase transformations that take place in AFMBs, and helping in the full understanding of the experimental findings.<sup>28</sup> In this regard, many studies concerning AFMBs complement experimental studies with computational ones using density functional theory (DFT) and/or *ab initio* molecular dynamic (AIMD) studies to fully understand the processes that take place and the effect of CC surface modification, SEI formation or electrolyte additive.

DFT is an atomistic first-principles modelling method used in physics, chemistry, and materials science to investigate the electronic structure of atoms, molecules, and condensed phases. It allows to calculate the energies of atomic structures and in order to gain a fundamental understanding of ion transport mechanisms, the electronic structure and its dynamics, thermodynamics, electron transfer, and various other properties in materials. In addition, first-principles calculations can be applied to predict new materials with little empirical input, as has been demonstrated for a wide range of battery, photovoltaic, thermoelectric, and catalyst materials.<sup>29</sup> Meanwhile, AIMD simulations have several advantages over other computational techniques. Compared to classical molecular dynamics (MD) simulations that model the real-time Newtonian dynamics of all atoms<sup>30</sup> in the materials using force fields that may not be readily available for the candidate material, AIMD simulations are chemically agnostic and are more suitable for studying new materials. In addition, the real-time ion dynamics of AIMD simulations allow direct observation of diffusion mechanisms without the need for *a priori* assumption about diffusion pathways. Therefore, AIMD simulations can be used to reveal diffusion modes within materials and to predict new fast ion-conducting materials.<sup>31</sup>

In general terms, the nucleation process that takes place in AFMBs is controlled by thermodynamic and kinetic factors. From the thermodynamic point of view, nucleation is governed

by the decrease in free energy due to the phase transition and the increase in surface energy because of the creation of a new interface. A higher value of binding energy can lead to a lower metal nucleation barrier and therefore to a lower nucleation overpotential. So, the binding energy values of the metal to the surface can be taken as a descriptor of the metal-philicity of the CC surface.<sup>27,32</sup> In general terms, the binding energies  $E_b$  of the atoms to the surface are calculated as:

$$E_b = E_{\text{subs+M}} - E_{\text{subs}} - E_M \quad (1)$$

where  $E_{\text{subs+M}}$  is the energy of the substrate plus the M atom,  $E_{\text{subs}}$  is the energy of the substrate alone and  $E_M$  is the energy of the M atom. Depending on the study,  $E_M$  refers to the energy of the isolated M atom or the energy of the M atom in the bulk M material.

For AFLMBs, lithiophilicity is one of the most important indicators to evaluate the quality of host materials when they are used as substrates for Li metal plating. Even though, there is not a direct way or formula to calculate the lithiophilicity, there are indirect ways used to evaluate it. A surface is called to be lithiophilic if it shows a good wetting towards Li-metal, *i.e.*, if it has a low contact angle with molten Li. For a homogeneous nucleation, ideally the interaction strength between CC and Li metal should be strong, *i.e.*, stronger than the interaction between Li and electrolyte and between individual Li atoms. A lithiophilic surface also requires a lower nucleation overpotential for Li metal plating compared to a lithiophobic surface.<sup>32</sup> Yan *et al.*<sup>33</sup> performed studies of Li plating on different metal surfaces. These authors deposited Li on two groups of metals. The first group consisted of the metals Pt, Al, Mg, Zn, Ag, and Au, which exhibit some solubility in Li. In the second group of metals, they considered Li plating on Si, Sn, C, Ni, and copper (Cu), which show negligible solubility in Li. They found that while the substrates of the former group yield a negligible overpotential for Li nucleation, this was not the case for the second group. This behavior was explained by the definite solubility of the substrate into the Li metal, which produces a solid solution buffering layer, previous to the formation of Li metal. Wang *et al.*<sup>34</sup> studied the electrodeposition behavior of Li plating on a Li<sub>2</sub>Te-Cu surface and compared it to the plating on a fcc Cu surface using DFT and electrochemical studies. They found that the monolayer plating of Li atoms on Li<sub>2</sub>Te-Cu is more stable than the formation of Li clusters, concluding that the electro-deposited Li film will be uniform. On Cu, however, the surface plating of three-dimensional (3D) Li islands is as stable as the Li monolayer plating, favoring in this way dendrite formation. Other surfaces like Li alloys were shown by Pande *et al.*<sup>26</sup> to present ideal characteristics for Li nucleation and surface diffusion. In this work, the authors found that the best-performing CC surfaces should possess Li adsorption energy close to zero to present a low activation energy of Li diffusion on the surface. The nucleation overpotential is determined by the adsorption free energy of Li on the CC surface and requires that the CC binds Li strongly. Shin *et al.*<sup>35</sup> demonstrated by DFT studies that Li adsorbs preferentially on Ag and AgLi than on Cu since Ag



forms an alloy with Li creating a homogeneous and smoother surface morphology. Cho *et al.*<sup>36</sup> also used Ag as a highly lithophilic material using Ag nanoparticles in polyethylenimine (PEI) as a stabilizing agent in the presence of LiNO<sub>3</sub>. They analyzed the system by DFT and AIMD and experimental studies finding that the Cu surface modification by Ag and PEI in the presence of LiNO<sub>3</sub> allowed for achieving a stable SEI surface controlling dendrite formation through a good nucleation process.

The nucleation rate  $J$  is a probabilistic process that is related to the free energy of formation of a critical cluster size  $\Delta G_{\text{crit}}$  according to:

$$J = Ae^{\frac{-\Delta G_{\text{crit}}}{kT}} \quad (2)$$

where  $A$  is a preexponential factor that depends slightly on the supersaturation. The meaning of  $\Delta G_{\text{crit}}$  corresponds to a maximum in the free energy of a cluster on a surface,  $\Delta G(N)$ , as a function of the number of constituent atoms  $N$ . by denoting  $N_{\text{crit}}$  the critical cluster size can be found that clusters with  $N > N_{\text{crit}}$  will grow spontaneously ( $\Delta G < 0$ ), while clusters with  $N < N_{\text{crit}}$  will dissolve spontaneously.  $N = N_{\text{crit}}$  corresponds to an unstable equilibrium.

For a cluster growing on a foreign surface the function  $\Delta G(N)$  can be written as:

$$\Delta G(N) = -Nze|\eta| + \sum_{i \neq j} \sigma_i A_i + A_{j*}(\sigma_j - \beta) \quad (3)$$

where  $z$  is the valence of the deposited ions,  $e$  is the electronic charge,  $\eta$  is the overpotential,  $A_i$  is the area of the  $i$ <sub>th</sub> face of the growing cluster and  $\sigma_i$  its specific surface energy.  $j^*$  labels the face of the cluster in contact with the surface, with the area  $A_{j*}$ , its specific surface energy  $\sigma_{j*}$  and the adhesion energy of the cluster with the surface  $\beta$ . The effect of a metaphilic surface on the nucleation rate in terms the parameter  $\beta$  in eqn (3) can be interpreted. A larger metal-philicity will imply a larger  $\beta$  and a negative shift of the free energy curve. Thus, for a constant overpotential  $\eta$ , this means a smaller critical free energy barrier  $\Delta G_{\text{crit}}$  and a smaller critical cluster size  $N$  for nucleation and growth. While this is a qualitative prediction, model calculations based on eqn (3) could be helpful to provide quantitative information.

In this sense, the metal-philicity of the different surfaces for different metals has been studied using first-principles calculation and will be discussed within each of them in the following parts. Broadly speaking, a review of the literature across various metals suggests that the efficacy of specific surface modifications or functionalization tends to be generalizable. In other words, a technique that proves beneficial for one metal is likely to demonstrate similar effectiveness when applied to other metals. As an example, the work of Chen *et al.*<sup>37</sup> can be considered that have studied the effect of doped carbon materials with the finding that O and boron (B) doping are the ones that will perform better as materials for AFSMBs and AFKMBs. They observed that Na and K present the same binding energy tendency on the doped carbon surfaces as observed in Fig. 2a

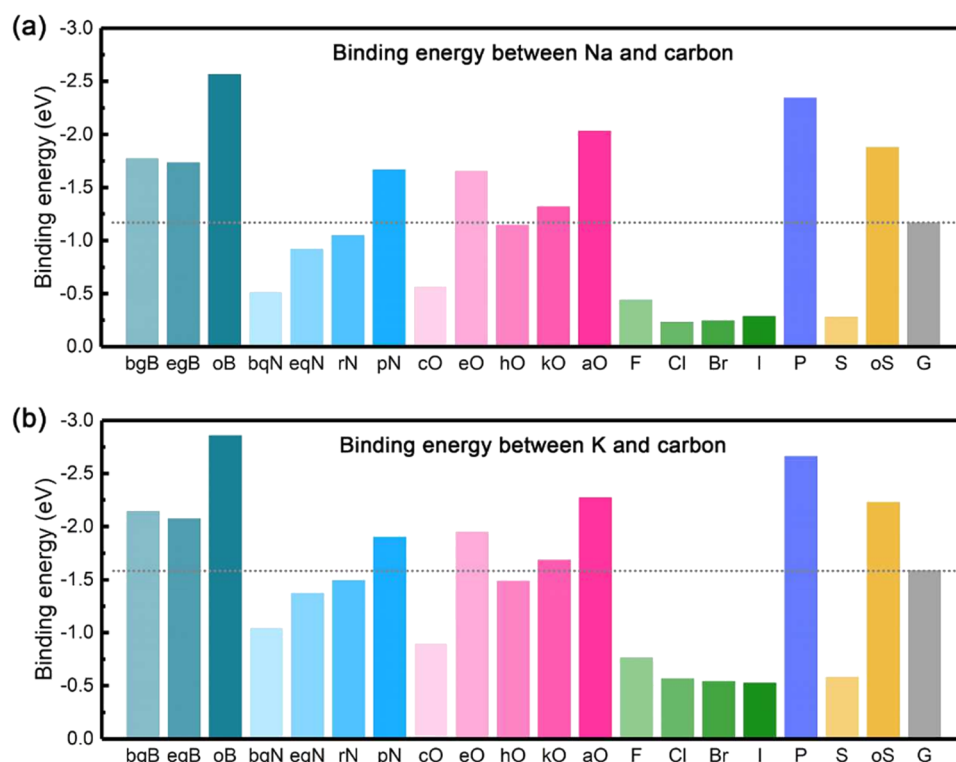


Fig. 2 The summary of binding energy on carbon materials: (a) the binding energy between Na and carbon, (b) the binding energy between K and carbon. Reprinted with permission,<sup>37</sup> Elsevier, Copyright 2020.



and b, respectively. They showed that apart from the presence of a carboxylic group (aO-doping); doping (bgB-, egB-), pyridinic N (pN-), epoxy (eO-), and ketone (kO-) doping are promising doping alternatives for practical design of three-dimensional carbon hosts taking in consideration the binding energy of Na and K on these surfaces.

Theoretical computational studies not only help to screen materials that potentially could be useful in the construction of anode-free CC, but also these tools play an important role in the understanding of the experimental results. These valuable tools allow us to gain an atomistic understanding of the interactions that take place between the surfaces of the CC and the metal-ions. Through these studies, it is possible to explore the energy barriers, the diffusion of atoms on the surface, and the reaction pathways helping in the understanding and designing possible new metalphilicity favorable surfaces. This last thing helps in the screening process of a wide range of materials, accelerating the discovery of the more promising ones. Computational studies such as DFT and AIMD are efficient and cost-effective tools that help to explore and understand the metalphilicity properties of different materials.

## 5. Anode-free Na-metal batteries (AFSMBs)

In recent decades, Na-ion batteries (NIBs) have attracted considerable attention as a potential complement to LIBs in both the academic and commercial sectors. The main reasons are the unbalanced geographic distribution of needed materials and the high cost of the elements required to make LIBs, such as Li, Co and Ni, which are not required to make typical NIBs. However, NIBs suffer from lower volumetric energy density as the anode materials are hard carbons, as an alternative, Na-metal batteries (SMBs) could provide higher energy density since Na (as the anode) is characterized by its high theoretical specific capacity of  $1165 \text{ mA h g}^{-1}$ . Nevertheless, the practical use of Na metal anodes has faced challenges related to non-uniform Na plating and the formation of an unstable solid electrolyte interface that degrades performance and reduces Coulombic efficiency (CE). In addition, issues such as dendrite growth pose safety concerns.<sup>38–41</sup> In response to these challenges, extensive efforts have been made to improve the stability and safety of SMBs, leading to research on AFSMBs. These batteries contain no active material, conductive materials, and binders in the anode electrode, reducing the cell weight and increasing the volumetric energy density, as only a CC is employed in the anode side.<sup>42,43</sup> In addition, the innovative design of a CC is the key factor to prevent the formation of dendrites during the plating/stripping processes. Safety concerns associated with traditional NIBs are mitigated due to the absence of a reactive Na-metal anode, eliminating risks of dendrite formation and short-circuiting. This section will not delve into electrolyte and SEI optimization for AFSMBs, as these topics have been covered extensively in recent literature.<sup>44–46</sup> In the following sections, the recent studies on CC modifications/

optimizations to overcome the challenges such as low CE, uniform and dendrite-free Na plating will be discussed, resulting in an enhanced AFMBs electrochemical performance.

### 5.1. CC optimizations

Cu-based CCs are frequently used for AFSMBs due to their excellent electrical conductivity, chemical stability, and compatibility with Na-ions. To overcome challenges such as the non-uniform plating of Na and the growth of dendrites on the CC surface, various strategies have been explored to improve the performance of Cu-based CCs in AFSMBs. For example, the formation of Na dendrites and the associated safety issues pose a challenge. To address this issue, Cheng *et al.*<sup>47</sup> have modified Cu foils with a bismuth (Bi) layer (Cu@Bi) that enabled controlled Na plating (Fig. 3a and b). The Bi modification layer exhibited excellent sodiophilicity, guiding the nucleation and growth of metallic Na. This property ensured a more uniform plating of Na metal, and reducing the formation of dendrites. Additionally, the Bi modification layer not only reduced the overpotential but also accelerated the reaction kinetics of Na metal plating/stripping. This could be attributed to the sodiophilicity of the Na–Bi alloy, which lowered the nucleation barrier and promoted efficient plating. As a result, the Cu@Bi CC demonstrated lower plating overpotentials compared to the bare Cu CC, indicating improved electrochemical performance, as the bare Cu CC exhibited a less conducive surface for Na plating, which caused an uneven distribution of current density and dendritic growth. The Bi modification layer also contributed to the formation of a stable and well-structured SEI on the surface of the Cu@Bi CC. The Bi modification layer stabilizes the SEI on the Cu@Bi CC by inducing uniform sodium metal deposition, forming a dense protective layer. This layer mitigates dendrite formation, reduces electrolyte consumption, and minimizes parasitic reactions for enhanced SEI stability. This SEI layer acted as a protective shield, preventing parasitic reactions and enhancing the stability of the Na metal anode during repeated cycling. The Cu@Bi CCs showed remarkable stability and efficiency during prolonged operation at various current densities.

The uniform plating of Na on the CC is essential for optimizing the performance, safety, and efficiency of anode-free Na metal batteries. To achieve this, Lee *et al.*<sup>48</sup> investigated the development of novel 3D nanostructured porous carbon particles with carbon shell-coated iron nanoparticles (PC-CFe) as a host for controlled Na metal growth in AFSMBs. The PC-CFe host was synthesized by carbonization of colloidal particles of nanostructured block copolymers, resulting in the formation of Fe nanoparticles coated with an ultrathin carbon layer (Fig. 3c). This hierarchical structure, which included sub-micrometer-sized carbon particles with ordered open channels and uniformly dispersed carbon-shell-coated Fe nanoparticles, enhanced cycling performance and demonstrated reversibility in Na plating/stripping operations. The PC-CFe's high efficiency is attributed to its 3D conductive network, which reduces energy loss, and its ultrathin carbon coating, which improves sodiophilicity and promotes homogeneous Na nucleation while



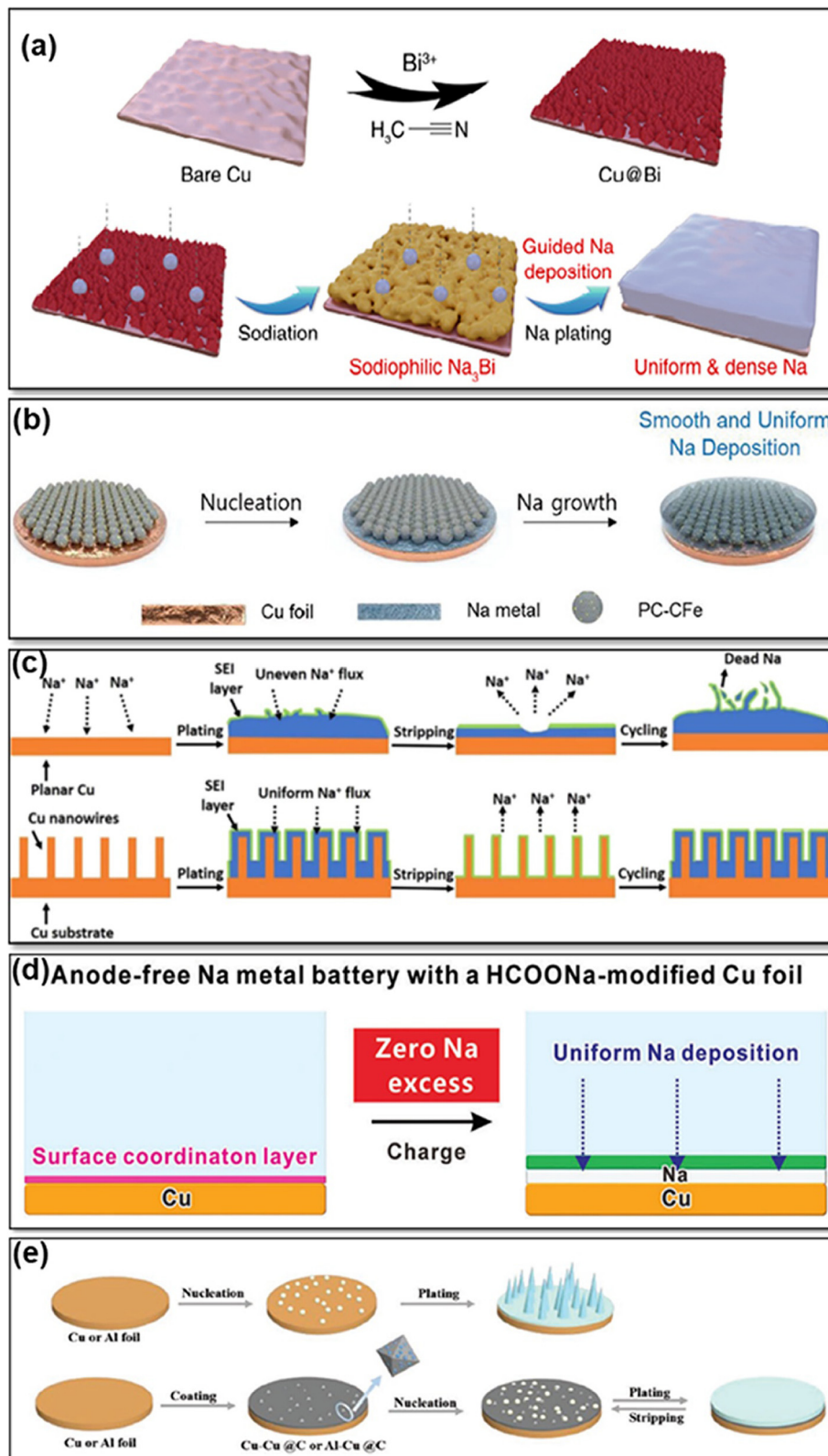


**Fig. 3** (a) Schematic representation of the Cu@Bi preparation process and Na plating on Cu@Bi surface. Reprinted with permission,<sup>47</sup> MDPI, Copyright 2023. (b) Schematic Illustration of uniform Na plating pattern on a Cu foil coated with PC-CFe. Reprinted with permission,<sup>48</sup> John Wiley and Sons, Copyright 2022. (c) Schematic Illustration of the Na plating mechanisms on both a planar Cu foil and a Cu NW-Cu substrate. Reprinted with permission,<sup>49</sup> Elsevier, Copyright 2018. (d) Illustration of Cu CC modified with the HCOONa. Reprinted with permission,<sup>50</sup> John Wiley and Sons, Copyright 2023. (e) Diagram depicting the plating of Na on untreated Cu or Al foils, contrasted with Cu@C or Al@C substrates. Reprinted with permission,<sup>51</sup> John Wiley and Sons, Copyright 2022.

limiting dendrite formation and successfully preventing oxidation. The hierarchical porous structure promotes efficient ion transport and accommodates volume fluctuations throughout cycle, increasing stability and lifespan.

Another notable contribution in this field was made by Wang *et al.*<sup>49</sup> who worked on the development of a CC that allows for uniform plating of Na-metal. Based on this, they introduced an approach by using a three-dimensional Cu-foam CC (CuNW-Cu) reinforced with Cu nanowires to enable reversible Na storage (Fig. 3d). Incorporating Cu nanowires onto a Cu foam CCs enhances its surface area, offering several benefits for Na plating. These nanowires act as abundant nucleation sites, promoting uniform Na deposition and mitigating dendritic growth. The increased surface area also reduces local current density, further suppressing dendrite formation. Experimental results demonstrate the CuNW-Cu CC's stability during prolonged cycling, ensuring the durability of sodium metal anodes. While direct sodium plating offers energy advantages, the CuNW-Cu design provided a practical solution by controlling nucleation and minimizing dendrite growth, enhancing the overall performance and safety of sodium metal anodes. In addition, the CC exhibited stability throughout prolonged cycling, showing minimal thickness variation. Furthermore, the EIS results indicated a significant reduction in charge transfer resistance for the Na@CuNW-Cu anode compared to the unmodified Cu CC. The lower charge transfer resistance of the Na@CuNW-Cu anode, compared to the unmodified Cu CC, is due to the increased surface area and uniform distribution of active sites provided by the *in situ* formed Cu nanowires. This suggested that the modified CC promoted efficient ion transport and electron transfer during the charge-discharge process. The improved kinetics contributed to higher CE and cycling stability, which are crucial for the long-term performance of Na-metal batteries.

An alternative method to improve the stability of Na plating/ stripping processes involves the use of 3D Cu nanowires with diameters of less than 40 nm, which was investigated by Lu *et al.*<sup>52</sup> They aimed to show how the unique structure of these nanowires can efficiently distribute the electric field, make a stable plating of Na-metal, and consequently suppress dendrite growth, which is a typical challenge in other planar CCs surfaces. The success of the study lies in the increased surface area of the 3D Cu structure through thinner nanowires, which stabilizes the Na plating by creating more nucleation sites. Importantly, testing has shown that thin-diameter 3D Cu nanowires are better at preventing dendrite growth than thicker wires (about 300 nm). Charge centers on electrode surfaces are crucial for uniform Na plating and dendrite prevention in MBs. Thin-diameter 3D Cu nanowires offer abundant charge centers due to their large surface area and inherent morphological features, promoting uniform Na plating by evenly distributing the electric field. While defects on flat Cu surfaces could also act as nucleation sites, the inherent roughness of these surfaces often leads to uneven plating. In contrast, the controlled, structured surface of 3D Cu nanowires enhances plating uniformity, mitigating the potential drawbacks of increased SEI

formation associated with larger surface areas. The stable plating behavior and good capacity retention observed with 3D Cu nanowires further underscore their efficacy in improving Na-metal battery performance. To avoid side reactions with electrolytes and the growth of dendritic Na deposits during (dis)charging cycles, a composite material derived from a Cu-based metal-organic framework (Cu@C), consisting of Cu nanoparticles integrated within a carbon framework (Fig. 3e) was proposed.<sup>51</sup> When applied to conventional Cu and Al CCs, Cu@C serves as a layer that promotes uniform Na plating by acting as a nucleus buffer. The Cu@C exhibited a high graphitic carbon content and reduced the nucleation barrier for Na plating on both Cu and Al CCs. *In situ* dilatometric measurements showed that the Cu@C nucleating film promoted the formation of dense metallic Na plating and suppressed the thickness growth caused by the accumulation of dead Na, which resulted in good cycling stability.

Al-based AFSMBs show significant promise due to their high energy density and cost-effectiveness. While Al is an attractive choice as a CC thanks to its abundance, light weight, and excellent conductivity, modifications are necessary to address challenges like metal-philicity, dendrite growth and cycling stability. Ongoing research focuses on enhancing aluminum foil's sodiophilicity and ensuring stable cycling performance, bringing these promising Al-based AFSMBs closer to practical applications in energy storage systems. Several research has revealed that carbon coatings can serve as nucleation sites for Na plating, considerably enhancing the performance of Na metal anodes. for example, Cohn *et al.*<sup>53</sup> demonstrated that a carbon film on an Al CC (C/Al) improved uniform Na plating, reduced nucleation overpotential, and increased mechanical stability. This resulted in a high CE of 99.8% over 1000 cycles and an energy density of approximately 400 W h kg<sup>-1</sup> (Fig. 4). Similarly, Dahunsi *et al.*<sup>54</sup> created nanosized carbon films on Al (C@Al), which resulted in a more homogenous Na plating procedure, lower overpotential, and better cycling stability, with over 99.5% CE and 93.0% capacity retention after 100 cycles. Furthermore, Cohn *et al.*<sup>55</sup> evaluated different nucleation layer compositions and discovered that carbon-coated CCs, whether hard carbon or carbon black, had lower nucleation overpotentials and higher electrochemical performance. These findings are applicable equally to Cu, highlighting the adaptability of carbon coatings in improving the sodiophilic characteristics and stability of Na metal anodes. Another work that investigated obstacles related to undesirable dendrite growth was conducted by Lee *et al.*<sup>56</sup> by developing a core-shell structure of silver nanofibers and nitrogen-rich carbon thin layers on Al CCs (SNF@NCL). The SNF@NCL nanohybrid structure can act as a catalytic template and improves Na ion nucleation by providing a high concentration of sodiophilic sites, promoting uniform metal deposition while reducing dendrite development. This leads to excellent cycling stability, with CE values exceeding 99% over long cycles. The combination of the conductive silver nanofiber core and the nitrogen-rich carbon layer promotes efficient electron transport and optimum Na ion interactions, increasing the performance of the battery.



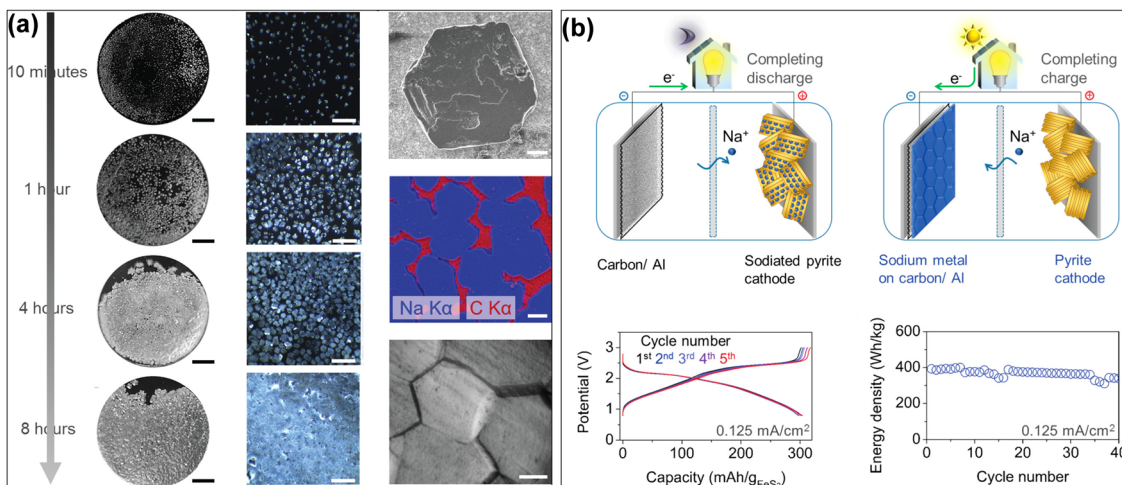


Fig. 4 (a) Photographs and micrographs of metallic Na on C/Al electrodes at  $0.5 \text{ mA cm}^{-2}$ , and also SEM and micrograph images of hexagon-shaped Na metal islands. (b) Schematic Illustration of the charge/discharge process of the C/Al CC (anode) with sodiated pyrite cathode in a AFSMB cell, and some electrochemical results. Reprinted with permission,<sup>53</sup> American Chemical Society, Copyright 2017.

To address the common challenges in Na plating/stripping, such as non-uniform deposition leading to dendrite formation, and low CE, researchers have investigated alternative CCs beyond conventional Cu or Al in AFSMBs. For instance, Wang *et al.*<sup>57</sup> created a 3D Ag@C cloth CCs as an efficient host for alkali metals by a simple thermal evaporation method to enable uniform Na plating. By pairing the Ag@C with a prussian white cathode, they showed a high initial capacity of  $133 \text{ mA h g}^{-1}$ , and the cells exhibited a capacity retention of around 56% after undergoing 800 cycles. Besides the sodiophilicity and nucleation sites of Ag@C, the good results can be also due to the smaller resistance created during Na plating/stripping cycles.

## 5.2. Computational studies of AFSMBs

By performing DFT simulations authors<sup>57</sup> found that Na atoms preferentially bind to Ag particles of the substrate being these sites sodiophilic and thus enabling a uniform plating. Also, by AIMD studies the authors found that Na moves away from the carbon surface towards Ag forming a Na–Ag network. Lee *et al.*<sup>48</sup> prepared 3D carbon-coated iron nanoparticles, FeNPs, (CFe) and evaluated the effect of the C coating using DFT calculations to compare the binding energy of Na on Cu (111), graphene, defective graphene surfaces, and CFe. They found that the nucleation of Na on pristine graphene is not favorable, but it is favorable in the presence of defects such as mono-, di- and tri- vacancy, and stone-wales defects, and the Na binding energy increases in the presence of Fe NPs serving as sodiophilic sites, lowering the nucleation energy barrier. The differential charge density studies showed that the presence of Fe under the graphene layer promotes Na adsorption by Fe NPs donating electrons between Na and graphene bond finding a good correlation between the Na energy binding and the amount of electron transfer of Fe in CFe atoms. The density of states (DOS) showed a strong hybridization between C 2p and Fe 3d near the Fermi level contributing to easier electron transfer. They also studied the effect of the amount of carbon

layers with the finding that there was a good Na adsorption on the carbon-coated Fe, which was maintained up to three layers, weakening sharply at four carbon layers and more. These findings helped in the understanding of the better-observed performance of CFe as anode-free for Na metals through the higher adsorption of Na on these materials due to the presence of Fe that acts as nucleation sites.

Liu *et al.*<sup>58</sup> performed DFT calculations with the finding that the simultaneous presence of functional groups containing O and N on a carbon matrix could regulate the Na adsorption on the surface in AFSMBs. The DFT calculation results helped to design 3D carbon-based nanofibers with sodiophilic O and N functional groups, which simultaneously facilitates homogeneous  $\text{Na}^+$  distribution, a dendrite-free construction, and reduces the plating overpotential. The sodiophilicity of 3D carbon fibers derived from polyacrylonitrile@zeolite imidazolate (PZC)<sup>59</sup> was experimentally and theoretically studied by means of DFT that observed that the presence of pyridinic and pyrrolic N and Zn sites within the carbon fiber host helped in the homogenous plating of Na decreasing the nucleation barrier. The study of electrolyte additives<sup>60</sup> has also been performed to attain a homogeneous Na plating by AIMD, helping in the design of a new electrolyte additive 1,2-dibromobenzene, which has the advantage of regulating the Na plating since it can decompose yielding sodium bromide increasing the Na diffusion across SEI layer.

## 5.3. Conclusion of AFSMB development

It is worth noting that a growing number of studies have focused on AFSMBs with optimized or modified CCs, particularly those based on Cu and Al. Strategies such as modifying Cu-based CCs with layers of metal nanoparticles or structuring them with three-dimensional nanostructured porous carbon particles have been found to enhance sodiophilicity, uniform Na plating, and improve CE and cycling stability. Similarly, Al-based CCs have been improved through approaches like thin



Table 1 Summary of CCs used in AFSMBs with used cathodes and electrolytes

CC	Cathode	Electrolyte	CE	Capacity retention	Capacity	Ref.
Cu-based	HCOONa	Na <sub>3</sub> V <sub>2</sub> (PO <sub>4</sub> ) <sub>3</sub>	1 M NaPF <sub>6</sub> in diglyme	99.7%	88.2% after 400 cycles	101.2 mA h g <sup>-1</sup> after 800 cycles at 2C
	3D Cu nanowires	Na <sub>3</sub> V <sub>2</sub> (PO <sub>4</sub> ) <sub>3</sub> /C	1 M NaPF <sub>6</sub> in DME	98%	99% after 200 cycles	92.5 mA h g <sup>-1</sup> at 0.5C
	Cu@Cl(5Na)	Na <sub>3</sub> V <sub>2</sub> (PO <sub>4</sub> ) <sub>3</sub> /C	1 M NaPF <sub>6</sub> in diglyme	99.9%	98.7% after 80 cycles	81 mA h g <sup>-1</sup> 1900 cycle at 5C
	CuNW-Cu	FeS <sub>2</sub>	1 M NaPF <sub>6</sub> in DME	97.5%	—	320 mA h g <sup>-1</sup> for 50 cycles at a current density of 0.2 A g <sup>-1</sup>
	PC-QFe	Na <sub>3</sub> V <sub>2</sub> (PO <sub>4</sub> ) <sub>3</sub>	1 M NaPF <sub>6</sub> in diglyme	—	97% after 100 cycles	49 mA h g <sup>-1</sup> at 2C
		Na <sub>3</sub> V <sub>2</sub> (PO <sub>4</sub> ) <sub>2</sub> F <sub>2</sub>	1 M NaPF <sub>6</sub> in DME	—	85% after 500 cycles	114 mA h g <sup>-1</sup> at 2C
		Na <sub>3</sub> V <sub>2</sub> (PO <sub>4</sub> ) <sub>3</sub>	1 M NaPF <sub>6</sub> in diglyme	99.2%	—	104 mA h g <sup>-1</sup> at 2C
		Na <sub>1.5</sub> VPO <sub>4.8</sub> F <sub>0.7</sub>	1 M NaPF <sub>6</sub> in diglyme	>99%	—	95.6 mA h g <sup>-1</sup> for 80 cycles at 1C
		Na <sub>3</sub> V <sub>2</sub> (PO <sub>4</sub> ) <sub>3</sub>	1 M NaPF <sub>6</sub> in diglyme	99.78%	95% after 100 cycles	108 mA h g <sup>-1</sup> at 0.1 A g <sup>-1</sup>
		Na <sub>2</sub> V <sub>2</sub> (PO <sub>4</sub> ) <sub>3</sub>	1 M NaPF <sub>6</sub> in diglyme	99.90%	82.5% after 100 cycles	300 mA h g <sup>-1</sup> after 3 cycles
Al-based	Cu@Bi	Na <sub>3</sub> V <sub>2</sub> (PO <sub>4</sub> ) <sub>3</sub>	1 M NaPF <sub>6</sub> in DME	—	>100 mA h g <sup>-1</sup> after 3 cycles	>100 mA h g <sup>-1</sup> after 3 cycles
	SNF@NCL	Na <sub>3</sub> V <sub>2</sub> (PO <sub>4</sub> ) <sub>3</sub>	1 M NaPF <sub>6</sub> in diglyme	99.85%	—	320 mA h g <sup>-1</sup> after 3 cycles
	Hard carbon	Na <sub>1.5</sub> VPO <sub>4.8</sub> F <sub>0.7</sub>	1 M NaPF <sub>6</sub> in diglyme	99.63%	—	>800 mA h g <sup>-1</sup> after 3 cycles
	Carbon black	Na <sub>3</sub> V <sub>2</sub> (PO <sub>4</sub> ) <sub>3</sub>	1 M NaPF <sub>6</sub> in diglyme	99.8%	—	>300 mA h g <sup>-1</sup> after 5 cycles
	Bi	Na <sub>3</sub> V <sub>2</sub> (PO <sub>4</sub> ) <sub>3</sub>	1 M NaPF <sub>6</sub> in diglyme	99.9%	96% after 30 cycles	87 mA h g <sup>-1</sup> after 1300 cycle at 5C
	Sn	Na <sub>3</sub> V <sub>2</sub> (PO <sub>4</sub> ) <sub>3</sub>	1 M NaPF <sub>6</sub> in diglyme	—	~93% after 100 cycles	—
	Carbon	pre-sodiated FeS <sub>2</sub>	1 M NaPF <sub>6</sub> in diglyme	—	56% after 800 cycles	136 mA h g <sup>-1</sup> after 3 cycles at 0.1C
	Cu@C	Na <sub>3</sub> V <sub>2</sub> (PO <sub>4</sub> ) <sub>3</sub> /C	1 M NaPF <sub>6</sub> in diglyme	94.1%	—	57 mA h g <sup>-1</sup> after 1000 cycles
	C@Al	Na <sub>3</sub> V <sub>2</sub> (PO <sub>4</sub> ) <sub>3</sub>	1 M NaClO <sub>4</sub> in EC/DEC/ FEC	99.9%	91% after 1000 cycles	61 mA h g <sup>-1</sup> after at 1C
	Ag@C cloth	Prussian white	1 M NaClO <sub>4</sub> in EC/DEC/ FEC	—	—	—
	Na <sub>2</sub> (Sb <sub>2/6</sub> Te <sub>3/6</sub> Vac <sub>1/6</sub> )	Na <sub>3</sub> V <sub>2</sub> (PO <sub>4</sub> ) <sub>3</sub>	1 M NaPF <sub>6</sub> in G2	—	—	—

carbon films, nucleation layers with varying compositions, and core–shell structures. These modifications have led to stable Na plating/stripping processes with dendrite-free growth. Some of the innovations discussed here not only contribute to improved energy density and reduced first-cycle losses but could also be promising for large-scale and cost-effective battery production. Exploring alternative CC materials, such as silver-coated carbon and metallurgical composites, has further widened the scope for AFSMBs. Using the modified/optimized CCs exhibit sodiophilic properties, enabling uniform Na plating and mitigating safety concerns associated with dendrite formation.

Computational studies, particularly DFT simulations, have provided valuable insights into the mechanisms behind Na plating and the interactions between Na and different CC materials. These simulations have aided in the design and optimization of CCs with improved sodiophilicity and reduced nucleation energy barriers.

There is a summary of CCs reported for AFSMBs in Table 1. So far, NVP family cathodes and electrolytes with NaPF<sub>6</sub> are commonly used in AFSMBs. As AFSMBs continue to develop, these advancements could offer reliable and sustainable energy storage solutions. The reported achievements in terms of cycling stability, energy density, and capacity retention, coupled with the exploration of novel materials and fabrication methods, highlight the potential of AFSMBs in revolutionizing the landscape of Na-battery technology. As these innovations continue to evolve, AFSMBs hold great promise for addressing the growing demand for high-energy-density, cost-effective, and environmentally friendly energy storage systems in the future. Upcoming researches may focus on further refining CC modifications, exploring novel electrolyte materials (solid, semi-solid and liquids), and integrating computational modelling to accelerate the development of next-generation AFSMBs.

## 6. Anode-free K-metal batteries (AFKMBs)

An all-metal-K anode has some great advantages over conventional anode materials such as graphite electrodes. Being composed of 100% active material, a metallic K anode has a relatively high theoretical specific capacity of 685 mA h g<sup>-1</sup>, corresponding to 586 mA h cm<sup>-3</sup>.<sup>62</sup> Furthermore, in non-aqueous electrolyte solvents, the electrochemical potential of K is even superior to that of Li and Na, indicating a higher operating voltage and energy density for a K-ion battery (KIB) system.<sup>63</sup> The reason for this lies in the weak interaction between K<sup>+</sup> ions and the solvent molecules of carbonate electrolytes, giving rise to a low desolvation energy and a small Stokes radius (compared to Li<sup>+</sup> and Na<sup>+</sup>). Thus, K<sup>+</sup> ions can easily strip off their surrounding solvent molecules and only need to overcome a small energy barrier to pass the SEI. The small Stokes radius also leads to a high ionic conductivity and fast ion transport which make KIBs promising for high-rate charging systems.<sup>62</sup> Last but not least, K with ~2.09 wt% is an abundant element in the earth's crust compared to Li

(~0.0017 wt%), enabling lower costs and greater market potential for rechargeable batteries.<sup>63</sup>

On the other hand, metallic K is inherently more reactive than metallic Li and must therefore be handled with greater care. Because K is so demanding in storage and handling, there is currently no K ribbon of defined thickness on the market, making it difficult to design reproducible experiments.<sup>63</sup> As K reacts violently with water, cell damage could have severe consequences and should be avoided at all costs. Additionally, K has a low melting point of ~63.5 °C, which is much lower than that of metallic Li (180.5 °C) and Na (97.8 °C). In the event of a thermal runaway of a K-metal battery, this can lead to the melting of solid K, further increasing safety issues.<sup>63</sup> The low melting temperature could on the other hand be useful to flatten the metal surface by annealing at elevated temperatures as a self-healing strategy. Summing up, the existing challenges of K-metal anodes appear to be more severe than those of Li-metal and Na-metal anodes. This is mainly attributed to the high reactivity of K, the large volume expansion effect, the unstable SEI, and the rapid growth of dendrites.<sup>63</sup>

AFKMBs avoid some of the disadvantages of K-metal by eliminating the need to handle pure K-metal during manufacture. For an AFKMB where each time the K is plated/stripped completely, it is of outmost importance to provide potassophilic nucleation sites to guarantee a homogeneous nucleation and growth of metallic K. This can, for example, be achieved by providing a mesoporous host-material<sup>64</sup> or a tissue with good wetting properties as compared with K as a CC.<sup>65</sup> To further homogenize the plating process Wang *et al.*<sup>66</sup> and Si *et al.*<sup>67</sup> introduced a carbon coating on the separator while Li *et al.*<sup>64</sup> and Tang *et al.*<sup>68</sup> tailored the SEI such, that dendrite growth was suppressed.

## 6.1. Functionalized CC and host-materials

To enable a homogenous nucleation of the K on the CC, it seems to be of outmost importance to tailor the surface energy of the CC to make it potassophilic. K has shown a good wetting on reduced graphene oxide<sup>66,67,69</sup> (Fig. 5a) and on other carbon-derived surfaces that possess a high defect density like NiO particles,<sup>70</sup> a graphene modulated defect-rich surface<sup>71</sup> or nitrogen-doped defects.<sup>64</sup> The contact angle of molten K on graphene and also the plating overpotential on graphene were reported to be reduced compared to graphite.<sup>71</sup> The wetting has also been enhanced on MXenes containing nitrogen, F-terminations, and a high defect density of Ti vacancies<sup>72</sup> as well as on an amine-functionalized surface giving a large amount of -NH sites at the surface.<sup>65</sup> The ammonia-functionalized carbon cloth of Meng *et al.*<sup>65</sup> showed a complete wetting within 4 s upon bringing the active carbon cloth in contact with molten K (Fig. 5b). In combination with a stable KF-rich SEI, they achieved a high cycling stability of 8000 cycles at 1 A g<sup>-1</sup> for an AFKMB full cell with a relatively low specific capacity of 80 mA h g<sup>-1</sup>, using the ammonia-treated carbon cloth as a CC (anode) and K<sub>0.7</sub>Mn<sub>0.7</sub>Ni<sub>0.3</sub>O<sub>2</sub> as a cathode with 0.8 M KPF<sub>6</sub> in EC:DEC (1:1) as electrolyte.

Zhao *et al.*<sup>71</sup> showed that a 150 nm thin coating of a defect-rich graphene-derived coating (Al@G) on an Al-CC showed a

low plating overpotential and a superior wetting and plating behavior when compared to a graphite coating (Al@C) and to the bare Al-CC (Fig. 5c–e). As a reason for the homogeneous film growth on Al@G Zhao *et al.* state that the surface energy of the Al@G substrate is much higher (66.6 mJ m<sup>-2</sup>) than the surface energy of the K metal resulting in the Frank-van der Merwe (F-M) mode (Fig. 5f). In contrast, if the surface energy of the substrate is low, like for the bare Al CC, the surface energy of the K metal determines the total energy of the system and the growth of isolated islands (*i.e.* dendrites) becomes energetically more favorable (Volmer-Weber (V-W) mode). The Stranski-Krastanov (S-K) growth mode describes the transition region and shows both characteristics, *i.e.* island growth on top of a closed film. Electrochemical impedance spectroscopy (EIS) analysis revealed the evolution of the charge-transfer resistance ( $R_{ct}$ ) during cycling of the differently functionalized CCs (Fig. 5g). The  $R_{ct}$  value for the Al@G interface was not only the lowest, it even showed a decrease during cycling (from 239 to 192 Ω) while the  $R_{ct}$  of Al@C and of the Al-CC showed a gradual increase. Zhao *et al.*<sup>71</sup> concluded that at the interface with the Al@G electrode a stable SEI was able to form that would not suffer from repeated cycling. This underlines that a smooth growth of K-metal is the key for a highly reversible plating/stripping and a high CE.

Due to the unstable nature of bare K metal and the large volume changes during plating/stripping, it is advisable to introduce a 3D host material that serves as a robust matrix for a homogeneous nucleation and growth of the K metal. An ideal host material should provide a robust structure that allows for good accessibility of all surfaces by the electrolyte. Hence, the porosity of the host material must not be too small. A large surface area would also lead to a huge consumption of electrolyte to build up the SEI. A macroporous structure, however, is often not able to withstand the electrode's volume changes.<sup>64</sup> As an answer to this, Li *et al.*<sup>64</sup> proposed a 3D mesoporous, carbonaceous fibrous film (called MCNF) that has a high mechanical strength. The MCNF is produced by pyrolysis of polyacrylonitrile (PAN) fibers embedded into a MOF. Its mesoporous structure of interconnected narrowly distributed pores allows for good ionic conductivity while having an overall surface area as low as 91.5 m<sup>2</sup> g<sup>-1</sup>.<sup>64</sup> The surface of the carbonaceous host possesses nitrogen-doped defects and is potassophilic. In combination with their optimized electrolyte Li *et al.* achieved an average CE of 99.3% for their MCNF||K half cells with an area loading of 3 mA h cm<sup>-2</sup> and a very good cycling stability under galvanostatic cycling with 3 mA cm<sup>-2</sup>.<sup>64</sup> A Full cell with a stable Prussian blue (PB) cathode (K<sub>1.81</sub>Fe[Fe-(CN)<sub>6</sub>]<sub>0.82</sub>·0.47H<sub>2</sub>O) against a MCNF matrix CC (as anode) was also demonstrated. The MCNF||PB cell achieved a high energy density of 362 W h kg<sup>-1</sup> at 20 mA g<sub>PB</sub><sup>-1</sup> for 100 cycles with a capacity retention of 86%.<sup>64</sup>

Potassophilic Pd/Cu CC was studied by Wang *et al.*<sup>73</sup> based on the selection of some potassophilic materials using first principles studies. Although the high cost of Pd, the choice was due to the binding energy of K on this material. A comparison with Cu showed that the Pd coating has a better potassophilicity than the original Cu foam. This leads to the reduction of



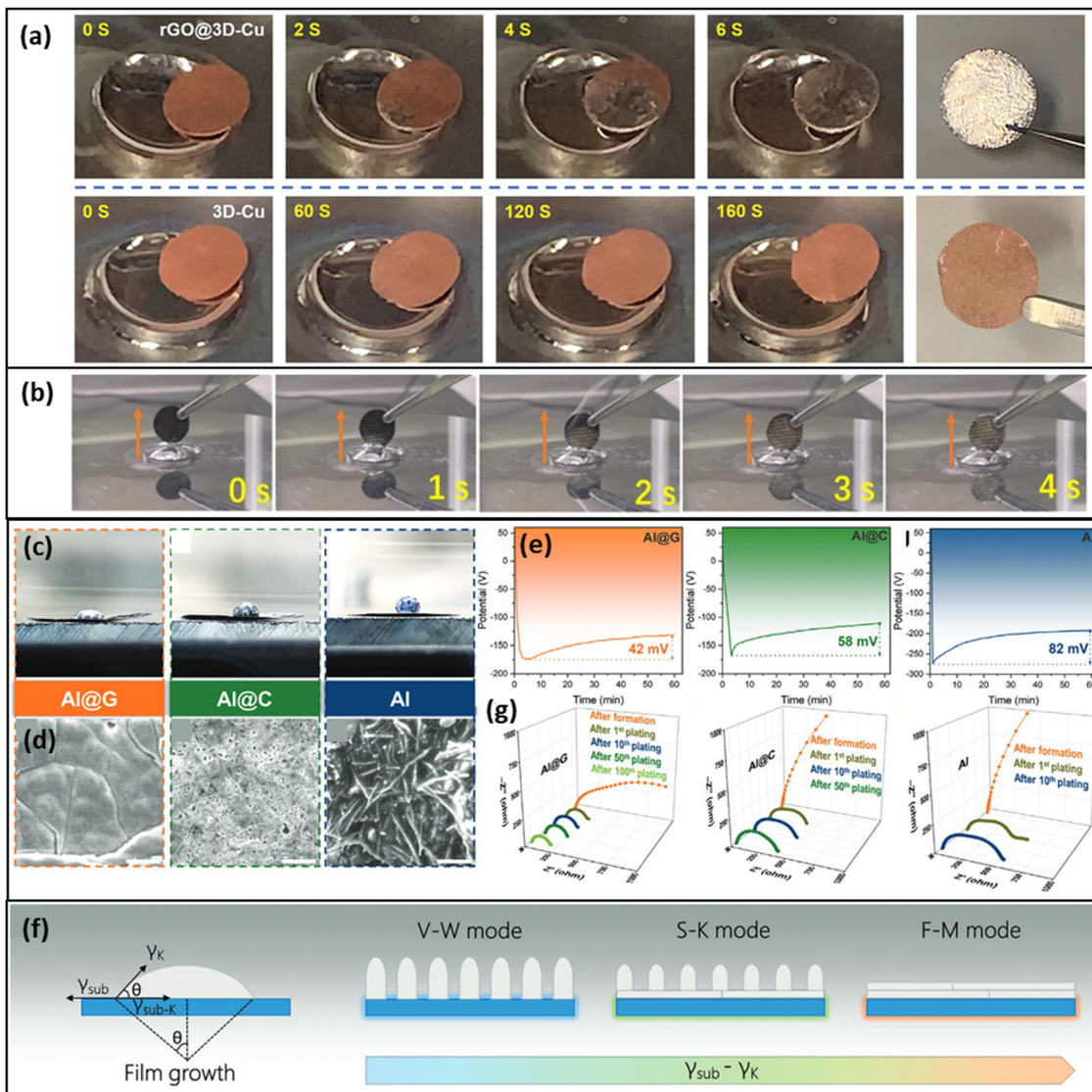


**Fig. 5** Demonstration of the potassiophilicity of a functionalized CC in contact with molten K metal. (a) A reduced graphene oxide (rGO) coating on a Cu CC leads to a complete wetting with molten K metal within 6 s, while the untreated Cu CC shows no K infusion at all. Reprinted with permission,<sup>69</sup> John Wiley and Sons, Copyright 2019. (b) An ammonia-treated carbon cloth CC shows complete K metal infusion within 4 s. Reprinted with permission,<sup>65</sup> American Chemical Society, Copyright 2022. (c) Wetting behavior of molten K on different CCs. (d) Top-view SEM images after 2.0 mA h cm<sup>-2</sup> of K plating, Scale bar: 10 μm. (e) First cycle overpotentials at 50 μA cm<sup>-2</sup> for the three CCs. (f) Schematic representation of film growth modes with respect to surface energy differences of film and substrate. (g) EIS Nyquist plots in the course of several cycles for the CCs Al@G, Al@C, and bare Al. Reprinted with permission,<sup>71</sup> John Wiley and Sons, Copyright 2019.

the overpotential of K<sup>+</sup> plating on Pd by effectively guiding the uniform K<sup>+</sup> plating and inhibiting the growth of K dendrites, finding a great correlation with the experimental results.

In general, AFKMBs can be built in combination with a variety of different pre-potassiated cathode materials such as potassiated prussian blue (KPB),<sup>64,74</sup> K<sub>0.51</sub>V<sub>2</sub>O<sub>5</sub>,<sup>67</sup> K<sub>0.7</sub>Mn<sub>0.7</sub>Ni<sub>0.3</sub>O<sub>2</sub> (KMNO),<sup>65</sup> 3,4,9,10-perylenetetracarboxylic acid-dianhydride (KPTCDA),<sup>68</sup> potassiated FeS<sub>2</sub><sup>71</sup> or cyanoperovskite K<sub>x</sub>MnFe(CN)<sub>6</sub>.<sup>75</sup>

## 6.2. Functionalized separator

The idea behind a functionalized separator is to introduce a layer through which the transport of the K<sup>+</sup> ions is diffusion-limited. This limitation will lead to a homogeneous

ion transport throughout the entire area of the separator. Si *et al.*<sup>67</sup> have shown that a coating of a glass fiber (GF) separator with reduced graphene oxide (rGO) can significantly improve the cycling stability of K plating/stripping on a Cu CC, and they stated that by regulating the K<sup>+</sup> flux the formation of dendrites is inhibited (Fig. 6). Furthermore, due to its K-philicity the rGO coating in contact with K-metal promotes the formation of a stable KF-rich SEI on the surface of the Cu CC which further contributes to smoothening the surface of the K-metal during plating/stripping. Liping Si and colleagues have previously stated that coating of the separator with rGO and LiNbO<sub>3</sub> particles leads to a homogeneous plating for K metal.<sup>66</sup> However, their latest publication<sup>67</sup>

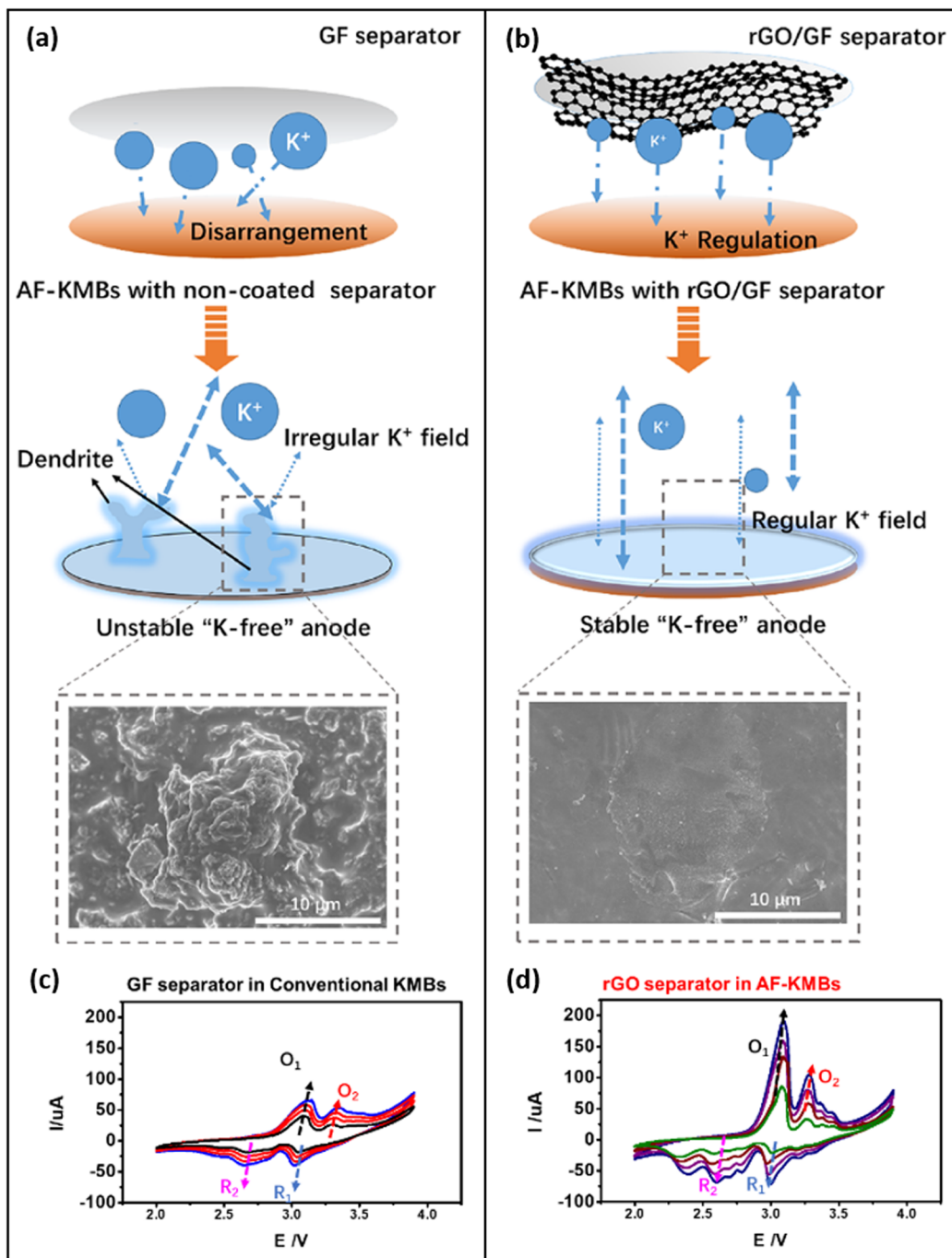


Fig. 6 Comparison between K metal plating with a standard glass fiber (GF) separator (a), with a GF separator functionalized with rGO (b). The functionalization with rGO leads to a homogeneous flux of  $K^+$  ions and a smooth K metal surface, while dendrites are formed without the rGO-functionalization. The rGO separator facilitates the reduction of  $K^+$  ions by improving the interface between the electrolyte and the metal surface, leading to increased peak currents during cyclic voltammetry (CV) (d) compared to the CV of an untreated GF separator (c). Reprinted with permission,<sup>67</sup> American Chemical Society, Copyright 2023.

suggests that the improved cycling stability is attributed to the rGO and not to the  $\text{LiNbO}_3$ . This group found an increase in the peak currents during cyclic voltammetry (CV) by the rGO-coated separator and they claim that the coating therefore increases the ionic conductivity of the battery (Fig. 6b and d).

To our understanding, the physics behind the positive effect on plating/stripping that was observed by Si *et al.*<sup>67</sup> is indeed different. The coating on top of the separator is unlikely to improve the ionic conductivity. In contrast, the rGO rather introduces a diffusion limitation that homogenizes local concentration gradients and hence the electric field. At the

same time, the transport of the  $K^+$ -ions through the KF-rich SEI is dramatically improved, leading to an overall increase in the peak currents during CV. In other words, besides the effect of homogenizing the ionic flux by building up a transport limitation through the rGO coating, the rGO could act as an artificial SEI that facilitates the removal of the solvation shell of the  $K^+$  ions and hence improves the cycling rate. rGO was also used by Liu *et al.*<sup>69</sup> for coating their 3D-Cu CC. As already mentioned in Section 6.1 (Fig. 5b) they found a good wetting of rGO with molten K after 6s, indicating that rGO is potassophilic.

### 6.3. Tuning of the SEI/electrolyte

A stable SEI that stays unchanged during cycling is crucial for achieving a high CE and long-term cycling stability. For KMBs, it turned out to be beneficial to have a strong and stiff SEI of mainly inorganic, ceramic nature that promotes the growth of a smooth metal surface without dendrite formation.<sup>62,74</sup> This is of course also true for AFKMBs where a stable SEI is of even greater importance for two reasons: just like a functionalized CC the backside of the SEI facing the CC can also serve as a nucleation site for K metal and therefore it can help to homogenize the plating result.<sup>67,68</sup> Additionally, if the SEI is not stable enough and breaks up or is partly dissolved during cycling, new SEI will form under consumption of  $K^+$  ions, which will directly decrease the battery capacity as K atoms are limited in AFKMBs compared to KMBs with a permanent stock of K metal. In the case of AFKMBs, a KF-rich SEI was found to improve the cycling stability.<sup>68</sup> Tang *et al.*<sup>68</sup> reported the use of polydimethylsiloxane (PDMS), a Si-O based additive in a non-aqueous low-concentration electrolyte of 0.4 M potassium hexafluorophosphate in 1,2-dimethoxyethane for AFKMBs. Using DFT calculations, they could understand the effect of PDMS on the plating behavior of  $K^+$  ions. They demonstrated that the presence of Si-O of PDMS modifies the electric field environment of the K-metal surface, which produces nucleophilic sites favoring uniform K-metal plating. Li *et al.*<sup>64</sup> suggested an inorganic bis(fluorosulfonyl)imide (FSI) anion-derived SEI which was also found to be beneficial for KMBs.<sup>62,74</sup> Li *et al.*<sup>64</sup> stated that the best performance was achieved with a 'diluted high-concentration electrolyte' (DHCE) which acts like a high-concentration electrolyte (HCE) but with a much lower K salt concentration. As a diluent, the hydrofluoroether TTE (1,1,2,2-Tetrafluoroethyl-2,2,3,3-tetrafluoropropyl ether) was used. The DHCE possesses like the HCE a low amount of DME in the coordination shell around the  $K^+$  ions and as in the case of the HCE, the degree of dissociation of the K salt is low, which favors the formation of an anion-derived SEI. Compared to the HCE, the DHCE preserves a high ionic conductivity and a low viscosity as well as a low K salt concentration which makes the DHCE less expensive. As K metal has a much lower shear modulus in comparison to Li and Na, a robust SEI might be able to exert enough pressure onto the K surface so that no dendrites can grow. If dendrite nuclei are not able to pierce through the SEI, they will stop growing. Tang *et al.*<sup>19</sup> produced a low-temperature AFKMB by using a KPF6/DME electrolyte and by introducing a

polydimethylsiloxane (PDMS) interlayer. The PDMS showed good wetting properties with the K surface and led to the formation of a robust hybrid SEI with organic K-O-Si-bonds and inorganic KF-based regions.

### 6.4. Summary of AFKMB development

It seems possible to get a good cycling stability and to suppress dendrite growth in AFKMBs by controlling the wetting at the interfaces and the nucleation and growth of the metal film (summarized in Table 2). The K plating can be homogenized in the following ways:

– A stiff and stable SEI that is mainly anion-derived and of an inorganic nature helps to keep the metal surface flat and suppress dendrites.

– Tuning the wetting properties, *i.e.* increasing the surface energy of the CC helps to achieve a homogenous nucleation. CCs with surface terminations like  $-OH$ ,  $-O$ ,  $-NH$ , and  $-F$  demonstrated a high potassophilicity, such as rGO (with an increased defect density compared to graphene), ammonia-treated carbons, and MXenes. Also, oxide materials such as NiO nanoparticles on the CC surface could serve as nucleation sites.

– Functionalizing a separator with rGO can limit the transport of the  $K^+$  ions and homogenize the ionic flux for a homogeneous plating of metallic K.

Due to the large volume changes (by molecular weight) compared to Li and Na, it is advisable to introduce a matrix as a nucleation site and as a space holder for the plating of K. Owing to its large atomic weight, K metal cannot compete with Li metal in terms of volumetric or gravimetric capacity. K ion batteries, however, can provide high energy and power densities and have the potential to become cheaper than LIBs. Hence, it is likely that KIBs will play an important role in stationary energy conversion systems. This is especially true for AFKMBs as during the manufacturing of the AFKMBs no handling of reactive K metal is needed. This will drop the costs and prevent any accidents with burning K metal during cell assembly. In addition, AFKMBs per definition can achieve greater energy densities than comparable KMBs.

## 7. Anode free Mg-metal batteries (AFMMBs)

There are several reasons why metallic Mg is a promising candidate for rechargeable metal batteries. In the first place, Mg has a large theoretical specific capacity, of 3833 mA h cm<sup>-3</sup> or 2205 mA h g<sup>-1</sup>, and a low electrode potential, of  $-2.37$  V *vs.* SHE.<sup>76</sup> A second advantage is the relatively large occurrence of Mg in the earth's crust, three orders of magnitude larger than that of Li, which is the current choice for state-of-the-art batteries. Mg has a lower chemical reactivity and a higher melting point (651 °C) than Li (180 °C), Na (98 °C), and K (63 °C), something which is important at the time of safety considerations. In addition, Mg-metal anodes are less prone to yield 1-dimensional (1-D) growth, leading to the formation of



**Table 2** The following table gives an overview of the functionalization methods and the corresponding battery performances for AFKMBs. Most of the methods aim to increase the surface energy of the CC by introducing defect and/or to increase the KF content of the SEI (for a better electric conductivity)

CC	Functionalization	Cathode	Electrolyte	CE	Capacity retention	Capacity	Ref.
Cu-foil	PDMS interlayer for low temperature use	KPTCDA	0.4 M KPF6-DME with 2 vol% PDMS	~98.9% at $-40^{\circ}\text{C}$	82% after 50 cycles	98.6 mA h g $^{-1}$ , (152 W h kg $^{-1}$ )	19
	Amine functionalized carbon cloth	$\text{K}_{0.7}\text{Mn}_{0.7}\text{Ni}_{0.3}\text{O}_2$	0.8 M KFSI in EC:DMC (1:1)	99.996%	68.5% after 8000 cycles	55 mA h g $^{-1}$ at $1\text{ A g}^{-1}$ after 8000 cycles at $-40^{\circ}\text{C}$	65
	Functionalized separator by rGO	$\text{K}_{0.51}\text{V}_2\text{O}_5$	3 M KFSI in DME	95.2% after 70 cycles	65 mA h g $^{-1}$ after 70 cycles	0.5 A g $^{-1}$	67
	Mesoporous carbo-naceous nitrogen-doped film (MCNF)	KPB	KFSI/DME/TTE (1/3/2 by mol)	99%	95% after 500 cycles	5.72 W h cm $^{-2}$ , 362 W h kg $^{-1}$ at 100 mA g $^{-1}$ <sup>GPB</sup>	67
	Titanium-deficient nitrogen-containing MXene/carbon nanotube freestanding scaffold rGO	Sulfurized polyacrylo-nitrile (SPAN)	0.8 M KPF6 in EC/DEC (1:1) 0.8 M KPF6 in EC/DEC (1:1)	99.2%	69.5% after 500 cycles	$\sim 312\text{ mA h g}^{-1}$ at 0.5 C	67
3D-Cu mesh	Defect-rich Al@G graphene-coating (high surface energy)	(K-FeS <sub>2</sub> )	4 M KFSI in DME	99%	K  Al@G: 4 mA h cm $^{-2}$ at 0.5 mA cm $^{-2}$ for 1000 h	71	
Al-foil							

dendrites. These differences are attributed to two facts:<sup>77</sup> On one hand, the free energy difference found for crystals with different shapes is more significant for Mg than for Li, thus favoring more compact structures.<sup>78</sup> On the other hand, Mg exhibits lower diffusion barriers than Li, thus enabling the structures to smoothen the surface after the nucleation process.<sup>79</sup> However, Mg electrodes are not immune to dendritic growth, as found by Kwak *et al.*<sup>80</sup> at current densities of  $10\text{ mA cm}^{-2}$  and above, so under extreme charging conditions, this is an issue that has to be taken into account.

The concept of anode-free batteries applied to Mg-metal has emerged relatively recently, to the point that the academic search on this topic with the keywords “anode-free Mg battery” yields references from the year 2021 onwards.<sup>81–87</sup> Similar to other metal-free arrangements, in an anode-free configuration, Mg<sup>2+</sup> ions are extracted from a fully pre-magnesiated cathode during an initial charging process. These ions are electrodeposited as metallic Mg on the CC, made of another material, which serves as a negative electrode for subsequent battery cycling. In the following sections, we discuss Mg electrodeposition on different CCs, which may be of great relevance to use as anodes in AFMMBs.

### 7.1. Mg electrodeposition on inorganic CCs

Based on the idea of magnesiophilicity, Li *et al.*<sup>88</sup> performed a conformal Au coating on a Cu CC using an ion-beam sputtering method and compared its behavior with that of a Cu CC upon Mg electrodeposition (Fig. 7a). While the Mg deposit on the Cu CC develops several cracks (Fig. 7b), a similar deposit on the Au-treated surface results in uniform and compact layers (Fig. 7c). A detailed study of Mg electrodeposition at lower capacities showed that the bare Cu electrode surface is initially covered by scattered micron-sized Mg lumps, which later merge into the large aggregates with cracks.

The superiority of the Cu–Au system is also reflected in electrochemical experiments with asymmetric cells with Mg||bareCu and Mg||Au–Cu electrodes (Fig. 7d). The cell with a bare Cu electrode presented sharp fluctuations in the CE curves, demonstrating a low CE at the first 25 cycles. In contrast, the Au–Cu electrode presented an initial CE of 89.42%, increasing to 99.88% in the second cycle and holding excellent behavior in the following 400 Mg plating/stripping cycles. As shown in Table 3, Au presents a larger magnesiophilicity than Cu, resulting in a stronger energy reduction during bonding. This contributes to homogenizing the Mg plating and suppressing “dead” Mg formation. The benefits of using magnesiophilic gold sites on different CCs were also demonstrated by Kwak *et al.*<sup>80</sup> They deposited diamond-shaped Au nanoseeds on different CCs (stainless steel (SS), Au treated SS, and Au treated Cu) using a sputtering procedure. While Mg plating on a Mg CC showed a nucleation overpotential of *ca.* 0.57 V at  $10\text{ }\mu\text{A cm}^{-2}$ , the presence of the Au nanoseeds on the Mg CC reduced this value to 0.43 V. Even at a high current of  $10\text{ mA cm}^{-2}$ , the Au nanoseeds were found to be effective in reducing the Mg nucleation overpotential on SS and Cu CCs. Under these high current conditions, in *operando* optical and

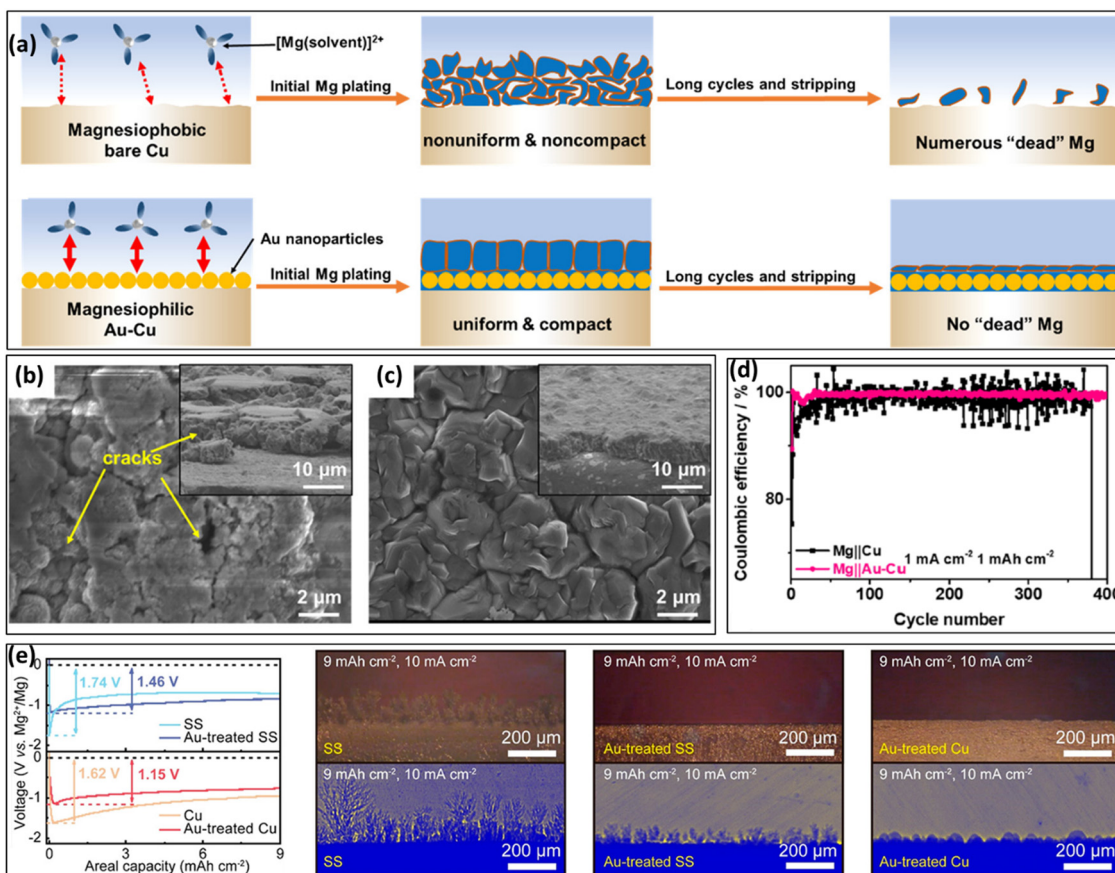


Fig. 7 (a) Schematic illustration concepts of the magnesiophilic bare Cu and Au–Cu CCs. SEM images of Mg deposit on (b) bare Cu and (c) Au–Cu CCs with a capacity of 2 mA h cm<sup>-2</sup>. (d) Cycling performances of the CE of Mg||Cu and Mg||Au–Cu asymmetric cells with a capacity of 1 mA h cm<sup>-2</sup> under 1 mA cm<sup>-2</sup>. Reprinted with permission.<sup>88</sup> American Chemical Society, Copyright 2022. (e) Comparison of galvanostatic profiles of Mg plating on different CCs, and also operando optical observations after Mg plating at 10 mA cm<sup>-2</sup>: stainless steel (SS), Cu and the same CCs treated with Au seeds. Reprinted with permission.<sup>80</sup> American Chemical Society, Copyright 2022.

X-ray observations showed that the Au nanoseeds prevented the occurrence of dendrites (Fig. 7e). In this way, the Au particles also delayed the short-circuit upon Mg plating compared with plating on a bare Mg surface. The compatibility of Mg and Au seems to be surprising when one starts to look for the physical reason. In principle, the bonding of Mg towards Cu should be energetically more favorable from the crystallographic point of view. Cu has a higher theoretical surface energy compared to gold and it can form alloys and interstitial phases with Mg. So, most likely the native oxide on the Cu CC which is not-existent on the more noble Au is changing the surface energy in a way that binding/wetting with Mg is less favorable. For the case of the Au nanoseeds, the mechanism might in fact rather be a physical functionalization. By introducing many tiny, highly conductive tips on the surface, the electric field is enhanced around these particles converting them into nucleation sites. Also, compared to a bulk material, nanoparticles do always have a high surface energy due to their large surface to volume ratio.

In principle, there may be several factors affecting the Mg growth mechanism on a foreign surface, like the gradients in electrolyte concentration, mechanical properties of the SEI,

relative surface energies of the metal involved, *etc*. The authors concentrated on two of them: the diffusion barrier of Mg atoms on the metallic substrate, and the binding energy of Mg atoms to the surface. A quantitative assessment can be made in terms of energetic considerations using DFT as a powerful tool. In Table 3, different binding energies for the interaction of a Mg atom with different substrates are shown. Depending on the references,  $E_{\text{Mg}}$  may be the reference of the isolated Mg atom or the Mg atom in the bulk Mg material. The latter is indicated with an asterisk on the Table 3. To relate both references, it may be considered that the cohesive energy of Mg is  $-1.50$  eV.<sup>79</sup> According to this table, for example, an Au(111) surface presents a considerably larger magnesiophilicity than a Cu(111) surface, since it presents a larger binding energy.

Kwak *et al.*<sup>80</sup> calculated by DFT the diffusion barriers for the motion of a Mg-ion to an adjacent site on Au(111), Cu(111) and Mg(0001). They pointed out that these values (0.033, 0.018 and 0.018 eV) were considerably lower than the diffusion barrier for a Li atom (0.14 eV), suggesting that this may be the reason why Mg is less prone to dendritic growth than Li metal.

Concerning the first of these factors, the discussion given in Section 3 can be addressed, where it was found that the barriers



**Table 3** Binding energy of Mg atom to different surfaces, as calculated using DFT in different articles according to eqn (1)

System: Mg atom on	Binding energy/eV	Ref.
Au(111)	-0.83 <sup>a</sup>	79
Cu(111)	-0.22 <sup>a</sup>	79
Au(111)	-2.01	79
Cu(111)	-1.61	79
Mg(0001)	-0.57	79
In(101)	-1.36	89
MgIn(001)	-1.56	89
In(101)	-0.81	89
Mg(002)	-0.75	89
Mg(001)	-1.12	90
MOF	-2.73	90
MgO(001) surface	-0.51	90
MgO(001) step	-1.26	
Cu(111)	-0.28 <sup>a</sup>	91
Mo(110)	-0.46 <sup>a</sup>	91
Mg(0001)	0.67 <sup>a</sup>	91
O-terminated graphene	-1.06 <sup>a</sup>	91
Graphitic, pyridinic, pyrrolic N at graphene	-0.03, -1.44, -3.23	91
C=O and -OH at graphene	-1.88, -1.33	91
M-Xene Ti <sub>3</sub> C <sub>2</sub> O <sub>2</sub>	-2.82	91
Ti <sub>3</sub> C <sub>2</sub> (OH)2, and Ti <sub>3</sub> C <sub>2</sub> F <sub>2</sub>	-0.73	
Ni(OH) <sub>2</sub> (110)	-0.33	
Ni(OH) <sub>2</sub> (002)	-1.89	92
Graphite	-0.57	92
Cu	-0.36	92

<sup>a</sup> Values refer to bulk Mg metal.

for Mg diffusion are considerably lower than those for Li diffusion, thus justifying why Mg is less prone to dendrite formation. As shown in Table 3, indium-containing surfaces should also show magnesiophilicity. For this reason, Yang *et al.*<sup>89</sup> used InCl<sub>3</sub> as an additive in magnesium triflate ((Mg(OTf)<sub>2</sub>)) in combination with 1,2 dimethoxyethane as a solvent. The test was performed in Mg||Al asymmetric cells. While the cells prepared using pure Mg(OTf)<sub>2</sub> electrolyte only lasted for 60 cycles, with a CE of 71.6%, the cells prepared with the InCl<sub>3</sub> additive endured 250 cycles, with an average CE of 98.7%. Besides the specific magnesiophilic effect, the presence of InCl<sub>3</sub> also resulted in improved reaction kinetics, as inferred from exchange current density measurements. The SEM measurements of deposits with and without the additive and finite elements simulations showed that the flat deposits obtained with InCl<sub>3</sub> yield a more homogeneous distribution of the electric field, in contrast with the surfaces without any additive, which yields a large electric field around sharp edges that lead to preferential plating on them.

Another example of the study of Mg plating on inorganic CCs can be found in the work of Bae *et al.*<sup>83</sup> They prepared a MgO-wrapped Zn-skeleton, which was used as a CC for Mg electrodeposition. To prepare these CCs, the surface of a Mg CC was scratched and immersed in a 1 M ZnCl<sub>2</sub> in tetrahydrofuran solution. Under these conditions, a chemical conversion reaction deposits Zn, while Mg<sup>2+</sup> ions are dissolved into the solution. As a consequence of this reaction, a 5 µm Zn layer appears on the Mg collector. Simultaneously, an ultra-thin layer (2 nm) of amorphous MgO appears on the Zn-skeleton. The

Magnesium plating reaction occurring on these structures leads to an interphase which is mainly composed of a MgO/Mg<sub>x</sub>O<sub>y</sub>/Mg mixture, subtended to a 6 nm region. Symmetric Zn-skeleton cells were assembled and their behavior was compared with that of Mg CCs. Upon cycling, the former presented an interfacial resistance reduced by a factor of 20.

While the bare symmetric Mg cells showed a rapidly increasing overpotential (1.58 V) due to the formation of a passivation layer on the Mg surface, the symmetric Zn-skeleton cell presents a very stable cycling performance with a considerably smaller overpotential (0.03 V). The authors attributed the good performance of the Zn Skeleton to the fact that the lattice mismatch between the Zn-skeleton and the MgO layer results in a very defective MgO layer, where the Mg<sup>2+</sup> ions may be rapidly transported, facilitating Mg plating. However, the authors did not appeal to the concept of magnesiophilicity in this work, for the sake of completion the binding energy of a Mg atom to Mg (001) surfaces and steps in Table 3 is added, which were found to be of -0.51 eV and -1.26 eV respectively. Since the authors point towards the occurrence of defective nanocrystalline MgO layers, the latter value should be rather considered for a measure of the magnesiophilicity of the surface. A Mg-Li hybrid battery prepared based on the Zn-Skeleton anode and a NMC (layered lithium-nickel-manganese-cobalt oxide) cathode endured 250 cycles at 0.5C and resulted in an energy density of 412.5 W h kg<sup>-1</sup> at 0.1C, which compares with the energy density of Graphite||NMC LIB.

The concept of magnesiophilicity also led Kwak *et al.*<sup>93</sup> to prepare Ag-decorated Cu foams (ACF) using a straightforward galvanic replacement procedure, by immersing a Cu foam (CF) in a 1.0 mM AgNO<sub>3</sub> solution. This led to the formation of Ag nanoparticles on the CF, resulting in a magnesiophilic surface with excellent behavior for Mg plating/stripping. The ACF CC reduced considerably the Mg nucleation overpotential at two different current densities.

## 7.2. Mg plating on carbon-containing CCs

Carbon cloth CC surfaces modified by  $\alpha$ -Ni(OH)<sub>2</sub> and  $\beta$ -Ni(OH)<sub>2</sub>, have also been used to improve Mg electrodeposition in Mg anode-free cells with a nucleation overpotential of -0.191 V compared with -0.491 V/-0.459 V for carbon cloth/Cu. Additionally, the modified CC showed better electrochemical cycling stability (Fig. 8a-d).<sup>92</sup> In this case, the improvement was discussed in terms of three concepts. On one hand, the concept of magnesiophilicity was discussed as in the previous case, but with the addition of two ingredients: lattice matching and electrostatic confinement effect. Further discussions for their results can be related to the fact that the binding energy of Mg to Ni(OH)<sub>2</sub> (110) and Ni(OH)<sub>2</sub> (002) surfaces (Table 3) is considerably larger than the binding energy of Mg to graphite and Cu. Thus, the larger magnesiophilicity of Ni(OH)<sub>2</sub> as compared with the magnesiophilicity of carbon and Cu explains the lower overpotential observed in the red curve of Fig. 8a. The other condition, that a small lattice mismatch favors epitaxial electrocrystallization of Mg on the CC, is also fulfilled in this case, since the geometrical deviation is about



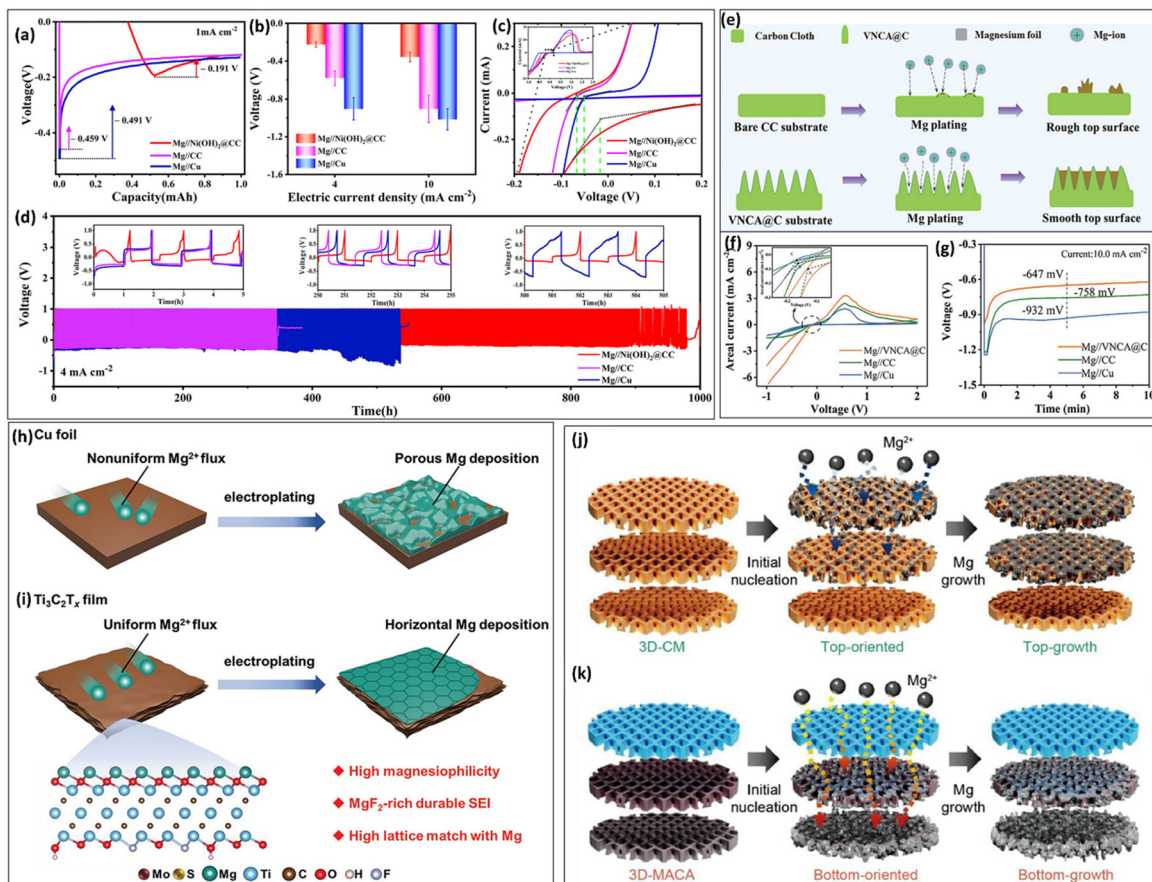


**Fig. 8** Overpotential of three asymmetric cells (Mg||Ni(OH)<sub>2</sub>@CC, Mg||CC, and Mg||Cu) at different current densities of (a) 1 mA cm<sup>-2</sup> and (b) 4 mA cm<sup>-2</sup>/10 mA cm<sup>-2</sup>. (c) Onset reduction potentials of cell CV curves at 1 mV s<sup>-1</sup>. (d) Electrochemical Mg plating/stripping profiles at 4 mA cm<sup>-2</sup>. Reprinted with permission,<sup>92</sup> American Chemical Society, Copyright 2022. (e) The schematic illustration of Mg electrodepositing on carbon cloth and VNCA@C (nitrogen- and oxygen-doped carbon nanofiber arrays on carbon cloth) CCs. (f) Cyclic voltammograms for Mg stripping/plating on the CCs. (g) Overpotential as a function of plating time for the galvanostatic plating on the CCs at 10 mA cm<sup>-2</sup>. Reprinted with permission,<sup>94</sup> John Wiley and Sons, Copyright 2021. (h) and (i) Schematic representation of Mg plating behaviors on Cu and Ti<sub>3</sub>C<sub>2</sub>T<sub>x</sub> MXene CCs. Reprinted with permission,<sup>87</sup> John Wiley and Sons, Copyright 2023. (j) and (k) Schematic illustrations of three-stacked Cu mesh (3D-CM) and the 3D Mg affinity-controlled architecture (3D-MACA) CCs and their Mg plating behaviors. Reprinted with permission,<sup>95</sup> Elsevier, Copyright 2023.

2.8% in contrast to the mismatch for Cu (20.9%) and for graphite (55.7%). Finally, the third concept introduced the alternate periodic arrangement of cations and anions of the Ni(OH)<sub>2</sub>@CC that would contribute to capturing and confining the Mg species, inducing a uniform Mg nucleation at the atomic level.

Lim *et al.*<sup>91</sup> have explored the use of a three-dimensional macroporous graphitic carbon nanosubstrate (GC-NS) for Mg plating. This GC-NS was prepared through thermal treatment of cellulose pellicles of bacterial origin, yielding a complex network structure, with many macropores. They compared Mg plating on GC-NS with the same phenomenon on Mo, Cu, stainless steel, and Mg as a CC. They found that the overpotential for GC-NS, (0.20 V) was considerably smaller than for Mo (0.27 V), Cu (0.53 V) and SS (0.43 V). Besides a better performance towards Mg nucleation, the GC-NS anode presented a larger affinity for the Mg deposit. The latter feature was derived from observations of the separator of the cell. While the system with the GC-NS anode presented a clean surface of the

separator after the plating of 5 mA h cm<sup>-2</sup> of Mg, the separators used with the other CCs were at least partially stained by the Mg metal. The calculations presented in Table 3 suggest that oxygen species terminating the CG-CS, which provide a binding energy of -1.06 eV relative to bulky Mg, may be responsible for the improved affinity of GC-NS for Mg.

Structures based on carbon nanofibers have also been used by Song *et al.*<sup>94</sup> in Mg anode-free cells for Mg plating, with the additional doping of N-species *via* polypyrrole nanofiber arrays on carbon cloth plating, which were carbonized at 800 °C in a nitrogen atmosphere to yield a cloth containing C (graphitic), N (pyridinic, pyrrolic, graphitic) and O(C=O, OH, O<sup>2-</sup>). This cloth was denoted with VNCA@C, to describe a Vertically aligned Nitrogen and oxygen-doped Carbon nanofiber array (Fig. 8e). Mg stripping/plating kinetics was investigated on these VNCA@C structures by cyclic voltammetry and galvanostatic transients uniformly electrodepositing metallic Mg, in comparison with the same process on carbon cloth and Cu CCs (Fig. 8f and g). All experiments were conducted in

all-phenyl-complex electrolytes.<sup>96</sup> While the voltametric profiles show that the VNCA@C electrode presents higher current responses during both cathodic and anodic sweeps as compared with those of carbon cloth and Cu electrodes (Fig. 8f) the galvanostatic transients for the former also show much lower overpotentials than for the other electrodes (Fig. 8g). The galvanostatic cycling performance of asymmetrical cells with Mg was tested at a current density of  $10.0 \text{ mA cm}^{-2}$ , and the Mg||VNCA@C could run for 40 hours with overpotentials of less than 0.5 V, but the other alternatives endured less than 5 hours with overpotentials over 1.0 V.

Besides the magnesiphilicity, a further factor that influences the Mg plating was the concavity of the surface on which this metal is deposited. A surface with periodically arranged concave structures would facilitate Mg nucleation on these sites by periodically enhancing the electric field strength and thus yield a smooth top surface. When many nuclei form and grow equally distributed on the surface, they will finally form a homogeneous film. In this respect, protrusions of Mg electro-deposits trigger the occurrence of large aggregates, as observed with carbon cloth and Cu foil (tip effect).

At the time of writing this review, the most recent work related to AFMMBs was that of Li *et al.*<sup>87</sup> who prepared MXene-based AFMMBs. They prepared 3D MXene ( $\text{Ti}_3\text{C}_2\text{T}_x$ ) films as a CC, where  $\text{T}_x$  represents the fact that the surface contains  $-\text{O}$  and  $-\text{F}$  containing terminations. A high magnesiphilicity, could be driven particularly by the oxygen terminations (Fig. 8h and i). This is mirrored in the large binding energy of Mg to  $\text{Ti}_3\text{C}_2\text{O}_2$  of  $E_b^{\text{Ti}_3\text{C}_2\text{O}_2} = -2.82 \text{ eV}$  (Table 3). This strong interaction and the small lattice mismatch of MXene with Mg leads to dendrite-free Mg plating. The estimated lattice mismatches of Mg (001) with  $\text{Ti}_3\text{C}_2\text{O}_2$ ,  $\text{Ti}_3\text{C}_2(\text{OH})_2$ , and  $\text{Ti}_3\text{C}_2\text{F}_2$  are 4.7%, 3.8%, and 3.8%, respectively. Fluorine terminations lead to the formation of a homogeneous and resistant  $\text{MgF}_2$  solid electrolyte interface layer. This is very important for inhibiting the consumption of Mg *via* a reaction with liquid electrolytes. Furthermore, the ( $\text{Ti}_3\text{C}_2\text{T}_x$ ) films provide a reasonable conductivity of  $4.69 \times 10^4 \text{ S m}^{-1}$  making it suited as a CC (Fig. 8i). At a large current density of  $5.0 \text{ mA cm}^{-2}$ , these electrodes run over 350 cycles with an average CE of 99.7%. In contrast, under analogous conditions a Cu electrode shows severe voltage fluctuations, collapsing after about 120 cycles.

### 7.3. Mg plating on structures with Mg controlled affinity

Recently, Kwak *et al.*<sup>95</sup> have proposed structures that present a gradient of magnesiphilicity as negative electrodes for AFMMs. The idea of this electrode, which is called a Mg affinity-controlled architecture (3D-MACA), is visualized in Fig. 8k. Since this idea could be extended to the engineering of other anode-free systems, we discuss it in some more detail. Three modified Cu meshes (CM), with different magnesiphilicities are stacked. The lower mesh is a CM modified with Au nanoparticles, and is denominated gold-decorated Cu mesh (GD-CD). This structure has a high magnesiphilicity, as discussed above. The mesh in the middle is obtained by thermal

treatment ( $180^\circ\text{C}$  and  $300^\circ\text{C}$ ) of  $\text{Cu}(\text{OH})_2$  nanofibers deposited on a Cu mesh, and has an intermediate magnesiphilicity. This layer is denominated heat-treated carbon mesh (HT-CM). The upper mesh is made of  $\text{Cu}(\text{OH})_2$  nanofibers deposited on a Cu mesh that was dried in a convection oven at  $80^\circ\text{C}$ , without further thermal treatment. This is denominated nanofiber-coated Cu mesh (NF-CM), and has a low magnesiphilicity. The behavior of this stack was compared with a similar stack, which consists of three layers of CM, without any treatment (Fig. 8j), denoted with 3D-CM.

The intermediate figures of Fig. 8j and k illustrate the nucleation and growth of Mg in the two types of architectures. While in the 3D-CM Mg is electrochemically deposited mainly on the top layer, since ions in the electrolyte find the shortest pathway, in the case of the 3D-MACA, the initial nucleation and subsequent growth take place in the bottom layer, which has the largest magnesiphilicity. This translates into the voltage-capacity behavior: While 3D-CM presents an overvoltage of  $0.214 \text{ V}$ , 3D-MACA this overvoltage is reduced to  $0.064 \text{ V}$ .

The different anodes were pre-deposited with Mg in a half-cell to  $1 \text{ mA h cm}^{-2}$ , then re-assembled into a full-cell in combination with the Chevrel phase as a cathode and cycled galvanostatically. The results showed that the 3D-MACA electrode presents an efficiency close to 100% up to 300 cycles, with capacity retention of about 80%. However, the 3D-CM electrodes showed a drop in capacity below 60%.

### 7.4. Electrolyte optimization

Especially for anode materials operating at low potentials, the SEI is a crucial component. In the case of metal anodes, a major problem of the SEI is its instability, mainly due to the large volume changes taking place during the charging/discharging processes. Mg-metal batteries have the additional downside that the SEI that is formed in electrolytes containing popular ions, like perchlorate and hexafluorophosphate in carbonate solvents, is impermeable to  $\text{Mg}^{2+}$  ions.<sup>97</sup> This problem is related to the high charge density of the  $\text{Mg}^{2+}$  ions and their small radius, leading to strong interactions with the materials where they diffuse. For this reason, electrolytes commonly used in Li batteries are inappropriate for the Mg-metal anode. For example,  $\text{Mg}(\text{PF}_6)_2$  did not attract much interest in Mg-metal batteries since the  $(\text{PF}_6)^-$  anion strongly passivates the surface of the Mg metal.<sup>98</sup>

There are excellent reviews discussing the choice of electrolytes for secondary Mg batteries, which in principle could also apply to anode-free Mg systems. For the work previous to 2019 the review of Deivanayagam *et al.*,<sup>97</sup> Ma *et al.*<sup>99</sup> and Attia *et al.*<sup>100</sup> can be addressed. A more recent review also addressing interphase issues has been given by Sun *et al.*<sup>101</sup>

In general, a plethora of electrolytes are viable for Mg metal batteries, however, the requirements of a large voltage window limits the practicality of many for battery applications. Among the articles revised for the present topic, by far the most used choice of electrolyte is the so-called all-phenyl complex (APC) in tetrahydrofuran (THF).



The first generation of electrolyte solutions was based on Grignard-type compounds.<sup>100</sup> They resulted from the reaction of organo-magnesium  $R_2Mg$  ( $R$  = alkyl or aryl group) with organic halo-aluminum compounds of the type  $AlCl_{3-n}R_n$ . In a suitable combination, this reaction yielded compounds with the formal composition  $Mg(AlCl_{4-n}R_n)_2$ , which were dissolved in THF or glymes.<sup>102</sup> While exhibiting an excellent electrochemical performance for Mg dissolution plating, it was found that they presented a relatively reduced electrochemical window of 2.4 V, which precludes its practical application in combination with some Mg-cathode oxides like  $V_2O_5$  and  $MoO_3$ .<sup>103</sup> The reason for this reduced electrochemical window was found to be the relatively weak Al-C bond of the electrolyte, that breaks *via* a  $\beta$ -H elimination in an electrochemical reaction.<sup>104</sup> Thus, the solution found by Mizrahi *et al.*<sup>96</sup> was to replace the R- aliphatic ligands with phenyl Ph-, which does not have a  $\beta$  hydrogen.

This proposal led to the so-called all phenyl complex (APC)-type electrolytes, which exhibit high anodic stability ( $>3.3$  V), low overpotential for Mg plating/stripping, and high CE. The second most used electrolyte was the magnesium trifluoromethane sulfonate ( $Mg(OTf)_2$ )-based electrolyte, where OTf represents  $SO_3CF_3$ , also denominated triflate. This compound was used with the addition of  $MgCl_2$  or  $InCl_3$ .  $Mg(OTf)_2$  has the advantages of being thermally stable, insensitive to ambient moisture, non-toxic, and available commercially with high purities.<sup>105</sup> The addition of  $Cl^-$  salts allowed the complete dissolution of the triflate into the 1,2-dimethoxyethane solvent, and the resulting solution outperformed the behavior of  $Mg(TFSI)_2$  (TFSI = bis(trifluoromethane)sulfonilimide).

### 7.5. Summary of AFMMB development

Although at its early stages, the development of AFMMB arrangements has very recently started with promising perspectives. The most widespread concept used in the literature is that of magnesiophilicity, which refers to the affinity of the CC for the Mg atoms being deposited, as compared with the affinity of Mg for itself. Evaluated from first-principles calculations, a high magnesiophilicity leads to epitaxial growth over dendritic one. Thus, calculations on different systems may be useful to select and/or design CCs. Connected to this is the diffusional barrier for Mg atoms on the CC. Lower barriers seem to favor the spreading of the atoms over the surface, thus preventing localized growth. Local electric fields are mentioned in the literature concerning two aspects: one referred to locking Mg atoms on fixed spots on the CC, which is an effect at a nanometric level. Another one referred to electric fields at a mesoscopic level, where a large electric field at tips may trigger dendritic growth. A small lattice mismatch between the CC and the growing Mg phase is also found to be positive for the quality of the growing interface. However, in some cases, defective structures, with many steps providing nucleation centers for Mg growth have shown to be useful for the present problem. Finally, the conductivity of the layer over which the Mg growth is achieved should also be evaluated to prevent resistive limitations.

## 8. Anode-free Zn-metal batteries (AFZMB)

Zn is a versatile and important metal in energy transition scenarios. A high theoretical capacity ( $820\text{ mA h g}^{-1}$ ), low cost, earth abundance and distribution, and environmental compatibility, are the main advantages of Zn in reversible battery devices. In recent years, research in this area has increased, particularly in the development of anodes for both aqueous and organic-based electrolytes. As it is the case for most metal anode batteries, an excess of metal drastically reduces the energy density.<sup>106</sup> Therefore, scientists and research groups are currently interested in developing AFZMBs to improve the energy density (zero excess Zn) by combining the environmental friendliness, high availability, and high cycling characteristics of these technologies for stationary energy storage, and smart grids. As the potential window of water as a solvent ( $\sim 1$  V) is limited by the water-splitting reaction, it is not possible to implement it in applications that require high power densities.<sup>106</sup> In this sense, AFZMBs in organic solvents are being developed, increasing the operating voltage.

As usual in metal-based batteries, the formation of dendrites is one of the main bottlenecks to be solved to ensure safety and reliability. Zn surfaces with (002) preferential orientation offer a series of advantages, mainly because they provoke a planar and dendritic-free plating of Zn.<sup>107</sup> There are different strategies to achieve this, such as interfacial layer, heterostructures, electrolyte composition, and metal surface modification with zincophilic structures, among others.<sup>106–108</sup>

### 8.1. Functionalized CC surface and host-materials

As is mentioned above, the most promising approach is to create zincophilic structures as a coating of the CC which induce (002) planar Zn nucleation. Xu *et al.* design a three-dimensional nano-Cu host modified by zincophilic antimony (Sb) nano-particles (ZA@3D-nanoCu) for AFZMB.<sup>109</sup> A full cell test was performed using  $MnO_2/Br_2$  as a cathode,  $TPABr_3 + ZnBr_2$  as the electrolyte, and ZA@3D-nanoCu as the anode. The battery was stable for 1000 cycles, showing a high specific capacity of  $400\text{ mA h g}^{-1}$  and an areal capacity of  $10\text{ mA h cm}^{-2}$  with a CE of 98.95%. The specific capacity is maintained even at high current densities. The modification of Cu with nanostructures capable of anchoring Sb zincophilic sites can induce desired Zn sites for homogeneous nucleation and stabilize the plating/stripping cycles.

Another zincophilic strategy to regulate Zn plating over a modified Cu-CC using Sb (Fig. 9a and b) has been proposed by Zheng *et al.*<sup>110</sup> The authors designed a  $Sb/Sb_2Zn_3@Cu$ -heterostructured interface as a CC for an anode-free Zn-Br<sub>2</sub> battery (Fig. 9c). They first studied the nucleation and growth of Zn over the modified  $Sb/Sb_2Zn_3@Cu$  surface using Zn foil as a counter electrode in a half-cell configuration, exhibiting a high stability over 700 h with an average CE of 97.8% and low overpotential of  $-20$  mV. The improved performance in comparison to the Cu||Zn asymmetric cell is attributed to the suppression of Zn dendrites by uniform, homogeneous, and



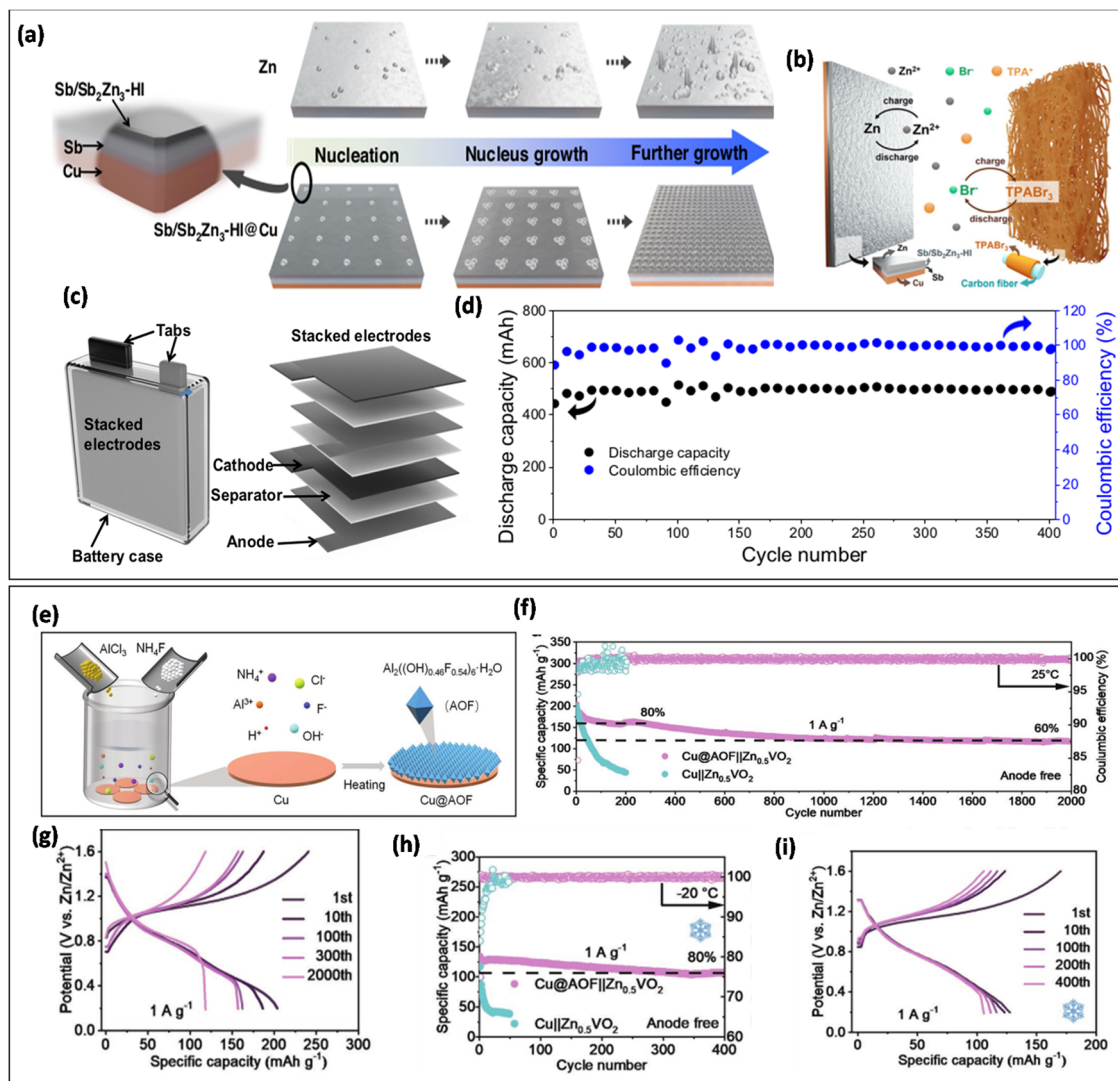


Fig. 9 (a) Scheme for the Zn nucleation and growth using Sb/Sb<sub>2</sub>Zn<sub>3</sub>@Cu modified and Zn foil. (b) Scheme for the full cell operation. (c) Scheme for the scaled-up cell applied to photovoltaic panel. (d) Capacity stability for the scaled-up cell. Reprinted with permission.<sup>110</sup> Springer Nature, Copyright 2023. (e) Scheme for the Cu@AOF synthesis and coating over Cu CC. (f)–(i) electrochemical results. Reprinted with permission.<sup>111</sup> John Wiley and Sons, Copyright 2023.

compact Zn electrodeposition without any discernible dendrites. After the excellent results in the half-cell, the full cell was built using Sb@Cu as an anode, carbon felt (CF) as cathode, ZnBr<sub>2</sub> and tetrapropylammonium bromide (TPABr) as the salts of an aqueous electrolyte. The authors first explored the rate capability and long-term cyclability. After cycling, the CC surface exhibited a dendrite-free morphology, indicating a homogeneous Zn nucleation given by the zincophilicity of the surface. Finally, this technology was scaled up (Fig. 9c) and connected to a photovoltaic cell panel as a battery module, resulting in an energy of 9 W h (6 V, 1.5 Ah) and 400 mA h g<sup>-1</sup> of specific discharge capacity over 400 cycles (Fig. 9d).

An additional Cu CC modification for an anode-free aqueous Zn battery has been proposed by Wang *et al.*<sup>112</sup> for room and low temperature operation. They synthesized and deposited Al<sub>2</sub>[(OH)<sub>0.46</sub>F<sub>0.54</sub>]<sub>6</sub>·H<sub>2</sub>O (AOF) on Cu foil (Cu@AOF) to guide the

Zn nucleation and suppress dendrite formation. The deposited AOF shows a high crystallinity, a strong binding with H<sub>2</sub>O molecules and a low diffusion energy for Zn adatoms which leads to good desolvation and fast diffusion processes on the surface, which drastically enhances layer-by-layer growth. The full cell setup was completed using pre-zincified VO<sub>2</sub> as a cathode, ZnSO<sub>4</sub> and Zn(OTF)<sub>2</sub> as the electrolyte, and Cu@AOF as an anodic CC. The asymmetric Zn||Cu@AOF half-cell showed a high cyclability of 6000 cycles at room temperature and 500 cycles at -20 °C. That is caused by a homogeneous, thin, and dense electrodeposition, as well as highly controlled plating/stripping processes which drastically inhibit the dendritic growth and side reactions such as ZnSO<sub>4</sub> formation on the CC surface and hydrogen evolution. The full cell ensemble displayed an initial specific capacity of 200 mA h g<sup>-1</sup> at 1 A g<sup>-1</sup> with 60% capacity retention after 2000 cycles at room

temperature, whereas  $140 \text{ mA h g}^{-1}$  at  $1 \text{ A g}^{-1}$  with 80% capacity retention after 500 cycles at  $-20^\circ\text{C}$  (Fig. 9e–i).

## 8.2. Dual Li-Zn Hybrid aqueous battery

Dual Li-Zn batteries usually involve Zn plating on the anode side and the simultaneous intercalation of other ions (*i.e.*  $\text{Li}^+$ ,  $\text{Na}^+$ ,  $\text{TFSI}^-$ ,  $\text{PF6}^-$ , *etc.*) on the cathode side. Thus, the cathode has a similar intercalation behavior to that of conventional LIBs, and the electrodeposition of  $\text{Zn}^{2+}$  occurs on the CC. However, excess of ions and highly concentrated electrolytes can cause corrosion of the CC surface, giving rise to various problems during the plating/stripping.

To improve the Zn plating on Cu CCs, Wang *et al.* proposed an anode-free Zn-graphite (ZGBs) dual ion battery with Cu protected with a thin layer (40 nm) of Ag as a CC and  $\text{Zn}(\text{TFSI})_2/\text{EMC}$  as electrolyte.<sup>107</sup> Thus, the  $\text{Zn}^{2+}$  deposits on the Cu@Ag CC by electroplating and the  $\text{FSI}^-$  intercalates into graphite cathode. The authors evaluated the system using half-cell and full-cell tests. Thus, they found an excellent behavior of the Zn plating/stripping process leading to a uniform Zn plating on Cu@Ag. They identified  $\text{AgZn}/\text{AgZn}_3$  alloys as zincophilic, which guides the subsequent dendrite-free Zn metal plating, and delivered a specific capacity of  $117 \text{ mA h g}^{-1}$ . In terms of full cell, the cycling was done under  $0.1\text{--}2.85 \text{ V}$  at  $0.1 \text{ A g}^{-1}$ . As a result, the full-cell ensemble presented a specific capacity of  $114 \text{ mA h g}^{-1}$  (based on the graphite mass in the cathode) with 82% capacity retention after 1000 cycles at  $0.5 \text{ A g}^{-1}$ .

Duan *et al.* developed an approach by controlling the reaction kinetics of the electrolyte in AFZMB using a Cu CC.<sup>113</sup> The authors proposed  $\text{LiFePO}_4$  (LFP) as cathode,  $\text{Zn}(\text{CF}_3\text{SO}_3)_2$  and  $\text{LiCF}_3\text{SO}_3$  as aqueous/Ethylene glycol (EG) electrolyte, and Cu foil as a CC. The presence of EG in the electrolyte provokes the uniform Zn plating and prevents the Zn dendrite formation thorough steric hindrance of  $[\text{Zn}(\text{H}_2\text{O})_m(\text{EG})_n]^{2+}$  complex, which retards the  $\text{Zn}^{2+}$  deposition.<sup>114</sup> The full cell LFP||Cu delivered an initial specific capacity of  $\sim 120 \text{ mA h g}^{-1}$  at  $1 \text{ mA cm}^{-2}$  with 75.2% capacity retention after 100 cycles.

In another recent study, An *et al.* designed a zincophilic robust heterointerface composed of 0D and 2D metal carbide nanosheets to adjust the Zn nucleation and growth for stable and homogenous Zn plating/stripping.<sup>115</sup> Thus, they synthesized an interface based on Na intercalated MXene  $\text{Ti}_3\text{C}_2\text{T}_x/\text{Sn}$  composite as a coating of the Cu CC (Cu@Na-MX@Sn). Herein, the rich O and F surface terminations of MXene likely anchor the Sn nanoparticles. The final surface has zincophilic sites distributed on it, favoring the (002) hexagonal Zn nucleation, avoiding the dendrite formation. The homogeneous Zn plating is probed at different rates and capacities. At current density of  $1.0 \text{ mA h cm}^{-2}$ , the Cu@Na-MX@Sn delivers stable CEs and long cycle life, whereas Cu@Na-MX shows a short-circuit after 129 cycles. The full cell was assembled with a  $\text{LiMn}_2\text{O}_4$  (LMO) cathode. The LMO||Cu@Na-MX@Sn cell showed a higher initial CE (71.2%) than LMO||Cu (42.1%). At a charging rate of  $100 \text{ mA g}^{-1}$  the specific capacity of LMO||Cu@Na-MX@Sn was  $50.09 \text{ mA h g}^{-1}$ , with a capacity retention of 73.97%,

whereas LMO||Cu delivered  $11.96 \text{ mA h g}^{-1}$ . The improvement is not only due to the zincophilic sites of Sn but also by the SEI stability given by  $\text{ZnF}_2$  and homogeneous electrical field provided by MXene.<sup>115</sup>

A similar approach was conducted by Chen *et. Al* who also used  $\text{Ti}_3\text{C}_2\text{T}_x$  as a robust heterostructure interface to control the Zn nucleation and growth.<sup>116</sup> The authors designed  $\text{Ti}_3\text{C}_2\text{T}_x/\text{nanocellulose}$  hybrid films with different weight percentages of  $\text{Ti}_3\text{C}_2\text{T}_x$ . The aqueous hybrid Zn-Li batteries were assembled with  $\text{Li}_2\text{MnO}_4$  as the cathode, a mixture of  $\text{Li}_2\text{SO}_4$ ,  $\text{ZnSO}_4$ , and  $\text{ZnF}_2$  as the electrolyte, and Cu coated by  $\text{Ti}_3\text{C}_2\text{T}_x/\text{nanocellulose}$  as a CC. In addition, they developed quasi-solid-state batteries using polyvinyl alcohol (PVA)/ $\text{ZnSO}_4/\text{Li}_2\text{SO}_4/\text{ZnF}_2$  hydrogel electrolyte. A specific capacity of about  $100 \text{ mA h g}^{-1}$  during 100 cycles at  $0.2 \text{ A g}^{-1}$  and  $60 \text{ mA h g}^{-1}$  at  $1 \text{ A g}^{-1}$  were obtained for the liquid electrolyte. Moreover, the full cell showed a lower nucleation overpotential with respect to the comparative hemi-cells. In the case of quasi-solid-state batteries, the full cell delivered a specific capacity of  $42.4 \text{ mA h g}^{-1}$  over 2000 cycles with a capacity retention of 81.5% at  $1 \text{ A g}^{-1}$ , corresponding to a gravimetric energy density of  $187.7 \text{ W h kg}^{-1}$  at a power density of  $181.2 \text{ W kg}^{-1}$  (based on the LMO mass) and a volumetric energy density of  $24.1 \text{ mWh cm}^{-3}$  at  $23.2 \text{ mW cm}^{-3}$  (based on the total volumes of two electrodes and hydrogel electrolyte). The demonstrated performance is associated with the synergist effect of the nanocellulose and  $\text{Ti}_3\text{C}_2\text{T}_x$  to improve the mechanical properties, electrical conductivity, and electrolyte wettability.

## 8.3. Computational studies of AFZMBs

In 2021 Zhou *et al.*<sup>117</sup> performed a theoretical and experimental analysis of the relationship between the surface structure and the interfacial reaction of the Zn anode. They found that on Zn (002), the Zn deposit initiated along the horizontal direction parallel to the sheet surface because of the stronger adsorption energy ( $-0.87 \text{ eV}$ ) between the (002) plane surface and Zn, compared to that of site 2 ( $-0.50 \text{ eV}$ ) maintaining a horizontal growth dendrite free Zn (002) surface. Nevertheless, on the Zn (100) plane, Zn preferentially nucleates at individual points (site 2) and subsequently grows vertically in a dendritic formation.

Yan *et al.*<sup>118</sup> studied the preferential growth of Zn (002) on Cu (100) obtaining a compact and planar-free dendrite anode. To demonstrate the preferential crystal orientation of Zn on Cu (100) they performed AIMD simulations and observed that the first Zn layer (underpotential plating of Zn on Cu) transforms from a hcp to a fcc crystal structure (close to the interatomic distance of Cu (100)). The first Zn layers that adopt the Cu (100) structure serve as a template for bulk Zn plating in a (002) direction inhibiting the growth of dendrites. Wang *et al.*<sup>119</sup> identified  $\text{AgZn}/\text{AgZn}_3$  alloys as a zincophilic phase that guides the subsequent dendrite-free Zn metal plating, and the cell delivered a specific capacity of  $117 \text{ mA h g}^{-1}$ . DFT calculations suggest that the trans-bis(trifluoromethanesulfonyl)imide anion ( $\text{TFSI}^-$ )-intercalated graphite is more stable than the *cis*- $\text{TFSI}^-$  intercalation compound by  $0.435 \text{ eV}$ . Also, by DFT



calculations An *et al.*<sup>115</sup> indicate that Sn (101) interacts effectively with Zn with a strong interfacial charge density. The electric field distribution modeled by COMSOL reveals that Na-MXene@Cu can homogenize the electric field and improve the wettability with ZnSO<sub>4</sub> electrolyte. MXenes are a kind of two-dimensional materials that consist of transition metal (M) atoms sandwiched between layers of carbon/nitrogen atoms. They are similar to graphene, but with the addition of transition metal atoms, which give them unique properties and possible applications in various fields of technology.<sup>120</sup> The improved electrochemical performance observed by Wang *et al.*<sup>112</sup> for aluminum hydroxide fluoride (AOF) coated on Cu foil was explained by DFT. The adsorption energies were obtained, giving as a result that AOF promotes the desolvation process of Zn<sup>2+</sup>. Binding energies showed that AOF favored a uniform Zn plating on the surface AOF.

#### 8.4. Electrolyte design.

The electrochemical performance of AFZBs can also be improved by electrolyte engineering. To avoid side reactions and mitigate the capacity fading An *et al.*<sup>121</sup> used multifunctional zinc fluoride (ZnF<sub>2</sub>) as an additive into the electrolyte to induce a stable F-rich interfacial layer. The authors investigated the effect of different concentrations of ZnF<sub>2</sub> in the electrolyte on the nucleation and side reaction of Zn on stainless steel as a CC. The nucleation and plateau overpotentials decrease significantly compared with the pristine 2 M ZnSO<sub>4</sub> aqueous electrolyte, indicating a lower resistance to Zn nucleation and deposition processes. The morphology of the Zn deposits showed a homogeneous surface when 0.08 M of ZnF<sub>2</sub> was added to the 2 M ZnSO<sub>4</sub> electrolyte, whereas an irregular particle distribution and dendrite shape was observed in pristine 2M ZnSO<sub>4</sub>. XRD postmortem analysis shows the accumulation of Zn<sub>4</sub>SO<sub>4</sub>(OH)<sub>6</sub>·H<sub>2</sub>O during the cycling in the case of the pristine ZnSO<sub>4</sub> electrolyte. In contrast, the amount of Zn<sub>4</sub>SO<sub>4</sub>(OH)<sub>6</sub>·H<sub>2</sub>O remains is practically negligible with the ZnF<sub>2</sub> additive. The full cell LMO||stainless steel assembly exhibited an improvement in the specific capacity and CE when ZnF<sub>2</sub> was used. In this way, F<sup>-</sup> species interfacing with the Zn surface may not only help to induce a homogeneous dendrite-free Zn deposition but also inhibit side reactions with the electrolyte interfaces.

Another interesting strategy is the design of co-solvent electrolytes. In this sense, Ming *et al.*<sup>122</sup> have proposed propylene carbonate (PC) and triflate anions in Zn(OTf)<sub>2</sub> aqueous electrolyte to form hydrophobic domains resulting in a solid electrolyte interface that avoids Zn dendrite formation and side reactions in a wide range of cathode materials. The salt effect is due to the amphiphatic effect of the OTf<sup>-</sup> anion; the hydrophobic -CF<sub>3</sub> group and the hydrophilic SO<sub>3</sub><sup>-</sup> group.<sup>123</sup> Using FT-IR spectroscopy, it was found that the presence of propylene carbonate (PC)/water mixture can regulate the coordination environment of OTf<sup>-</sup> anions by forming a [PC-Otf-H<sub>2</sub>O] complex. In terms of electrochemistry, the authors studied the compatibility of the hybrid electrolyte with different cathodes in the full cell set-up at a low rate of 50 mA g<sup>-1</sup>, finally choosing the Zn-rich ZnMn<sub>2</sub>O<sub>4</sub> cathode to avoid complicated and time-consuming pre-zincification reactions. The anode-free Cu (CC)|| ZnMn<sub>2</sub>O<sub>4</sub> with Zn(OTf)<sub>2</sub> in propylene carbonate/water as electrolyte showed a high capacity retention of 80% after 300 cycles.

In other study, Duan *et al.* developed an approach by controlling the reaction kinetics of the electrolyte in AFZMB using a Cu CC.<sup>113</sup> The authors proposed LiFePO<sub>4</sub> (LFP) as cathode, Zn(CF<sub>3</sub>SO<sub>3</sub>)<sub>2</sub> and LiCF<sub>3</sub>SO<sub>3</sub> as aqueous/Ethylene glycol (EG) electrolyte, and Cu foil as a CC. The presence of EG in the electrolyte provokes the uniform Zn plating and prevents the Zn dendrite formation through steric hindrance of [Zn(H<sub>2</sub>O)m(EG)n]<sup>2+</sup> complex, which retards the Zn<sup>2+</sup> deposition.<sup>114</sup> The full cell LFP||Cu delivered an initial specific capacity of ~120 mA h g<sup>-1</sup> at 1 mA cm<sup>-2</sup> with 75.2% capacity retention after 100 cycles.

#### 8.5. Summary of AFZB development

Table 4 summarizes the main results of the strategies for AFZBs. The CC coating is one of the most important problems to be solved in AFZBs. The appropriate modification of the CC by zincophilic species, such as nanoparticles and heterostructures, and the electrolyte formulation with amphiphilic salt and organic/water-based solvent are emerging as promising strategies to selectively induce the hexagonal (002) Zn nucleation and growth. That can help to homogenize the electric field, and prevent the formation of dendrites, showing specific capacities and energy densities suitable for renewable energy storage probed in solar cell integrated grids.

**Table 4** Summary of composition and electrochemical properties for the different AFAZBs. VW = voltage window, SC = initial specific capacity, CR = capacity retention

Cu coating CC	Electrolyte	Cathode	VW/V	SC/mA h g <sup>-1</sup>	CR/cycles	Current Density	Ref.
@Ag	Organic: Zn(TFSI) <sub>2</sub> /EMC	Graphite-Zn	0.1–2.8	114	82%/1000	0.5 A g <sup>-1</sup>	107
@Polyvinil Pyrrolidone	Aqueous: ZnI <sub>2</sub> , I <sub>2</sub> , ZnSO <sub>4</sub>	ZnI <sub>2</sub>	0.6–1.6	150	64%/200	1 A g <sup>-1</sup>	124
@Carbon nanodisc	Aqueous: Zn(CF <sub>3</sub> SO <sub>3</sub> ) <sub>2</sub> , Mn(CF <sub>3</sub> SO <sub>3</sub> ) <sub>2</sub>	MnO <sub>2</sub>	0.8–1.8	200	69%/80	1 A cm <sup>-2</sup>	125
—	Aqueous/EG: Zn(CF <sub>3</sub> SO <sub>3</sub> ) <sub>2</sub> , LiCF <sub>3</sub> SO <sub>3</sub>	LiFePO <sub>4</sub>	0.6–1.6	120	75%/100 cycles	1 mA cm <sup>-2</sup>	113
@Mxene-Ti <sub>3</sub> C <sub>2</sub> T <sub>x</sub> /Sn	Aqueous/ZnSO <sub>4</sub>	LiMn <sub>2</sub> O <sub>4</sub>	1.4–2.1	50	50%/	100 mA g <sup>-1</sup>	115
@Ti <sub>3</sub> C <sub>2</sub> T <sub>x</sub> /nanocellulose	Aqueous/Li <sub>2</sub> SO <sub>4</sub> , ZnSO <sub>4</sub> , ZnF <sub>2</sub>	LiMn <sub>2</sub> O <sub>4</sub>	1.4–2	60	86%/2000	1 A g <sup>-1</sup>	116
@Ti <sub>3</sub> C <sub>2</sub> T <sub>x</sub> /nanocellulose	Aqueous-PVA/Solid State Li <sub>2</sub> SO <sub>4</sub> , ZnSO <sub>4</sub> , ZnF <sub>2</sub>	LiMn <sub>2</sub> O <sub>4</sub>	1.4–2	42	82%/2000	1 A g <sup>-1</sup>	116
@Cu 3D-nanostructured	Aqueous/ZnBr <sub>2</sub> , ZnSO <sub>4</sub>	MnO <sub>2</sub> /Br <sub>2</sub>	0.6–1.6	450	89%/1000	10 mA cm <sup>-2</sup>	109
@Sb/Sb <sub>2</sub> Zn <sub>3</sub>	Aqueous/ZnBr <sub>2</sub> , TPABr	Br <sub>2</sub>	0.5–1.6	220	95%/40	20 mA cm <sup>-2</sup>	110
@Al <sub>2</sub> (OH) <sub>0.46</sub> F <sub>0.54</sub> ) <sub>6</sub> ·H <sub>2</sub> O	Aqueous/ZnSO <sub>4</sub> Zn(OTf) <sub>2</sub>	Zn <sub>0.5</sub> VO <sub>2</sub>	0.3–1.6	200	60%/2000	1 A g <sup>-1</sup>	111



The scalability and application in real systems are still at an early stage in terms of engineering, design and development. At present, the processes such as the synthesis/deposition of the nano-heterostructures and the pre-zincification of the cathodes, are not easily transferable to an industrial scale. Nevertheless, these problems can be overcome in the near future.

## 9. Anode-free Al metal batteries (AFAMBs)

Al-ion batteries (AIBs) have great potential due to their high theoretical specific capacity (gravimetric capacity:  $2980 \text{ mA h g}^{-1}$ , volumetric capacity:  $8040 \text{ mA h cm}^{-3}$ ), the abundance of Al in the earth's crust, and good safety. The predominant bottleneck for the commercialization and therefore the primary focus of research is the cathode material, to which most of the failure mechanisms are attributed.<sup>126</sup> However, the Al anode shows low stability and reversibility due to hydrogen evolution in aqueous electrolytes, dendrite growth, and the formation of a passivation layer of  $\text{Al}_2\text{O}_3$ , which hinders or even prevents the oxidation of the Al to free  $\text{Al}^{3+}$  ions depending on the electrolyte.<sup>127</sup> To date, most AIBs use chloroaluminate-based electrolytes due to their ability to reduce the native oxide layer and their high oxidation and reduction power for Al. The downsides are the possibility of the formation of highly toxic chlorine gas and that chloride-based systems corrode most CCs, limiting the choice of the CC to graphite paper or more expensive materials such as molybdenum or titanium.<sup>128</sup> This drastically reduces the degrees of freedom for an anode-free approach. Electroplating in general is a process that is strongly influenced by the interfacial properties of the substrate and the amount, size, and crystal orientation of nucleation seeds.<sup>106,108,129</sup> This means that anode-free approaches offer great potential in terms of tunability, but also increase the complexity and price of such batteries.

### 9.1. Comparison of various current collector materials

Wang *et al.* investigated eight different anodic CCs, including Al, Molybdenum (Mo), Cu, Ag, Ni, Mg, stainless steel (SS), and graphite paper (GP) for AFAMBs with a GP as a cathode and also

as a cathodic CC, and  $\text{AlCl}_3/[\text{EMIm}]\text{Cl}$  as the electrolyte.<sup>128</sup> Metals susceptible to corrosion by  $\text{Cl}^-$  such as Cu, Ag, Ni, or Mg have a low initial CE (ICE) of about 50% to 60% and a low average CE of around 95% (Fig. 10a). Once the electrolyte is reduced to a certain extent, a rapid fading of the capacity is observed. The CE of the cells/electrodes made with SS CC increases with subsequent cycles up to 98% where it stabilizes, indicating the formation of a stable passivation layer. It should be noted that excessive amounts of electrolyte were used for these tests, so larger amounts of electrolyte may be needed to compensate for the losses until the cell stabilizes. Mo and GP CCs, which are resistant to  $\text{Cl}^-$  corrosion, show high ICES of 98,7% and 92,1%, respectively, and an average CE above 98% during subsequent cycling. Although the loss mechanisms were not further elucidated, the formation of stable deposits that cannot be stripped due to a high surface energy is likely to be the reason in the initial cycle.<sup>130</sup> This conclusion is supported by Fig. 10b, where clear clusters are visible on some electrodes in SEM and EDX images of a fully discharged cell with a Mo CC after 100 cycles. Since the cathode of all batteries is GP, cathodic reactions are unlikely to be the cause of the differences in the ICE. Plating of Al metal on the surfaces of the electrodes was confirmed with XRD analysis, which indicated the proportion of (111) and (200) Al deposits. The GP as anodic CC results in a homogeneous layer of plated Al with some particles forming on the surface (Fig. 10c). Due to the low surface energy of graphite, it generally shows poor wettability.<sup>71</sup> Aluminophilicity might be achieved by increasing the density of defects at the interface and thereby reducing the overpotential of the electrochemical reaction. The metals used for the different electrodes were purchased and used directly as the CC without further modification, except for the GP anodic CC, which was calcined in Ar at  $1000^\circ\text{C}$  for 3 h. Therefore, it is possible that surface modification or the use of monocrystalline metals can strongly increase plating and stripping efficiency.

### 9.2. Functionalized CC surface

In 2020, Zhao *et al.*<sup>127</sup> first demonstrated the importance of the lattice mismatch between the CC and the Al on the

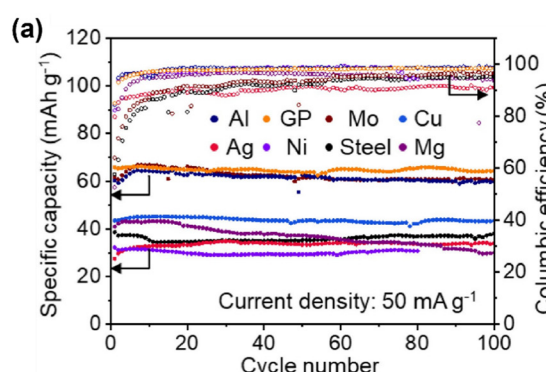
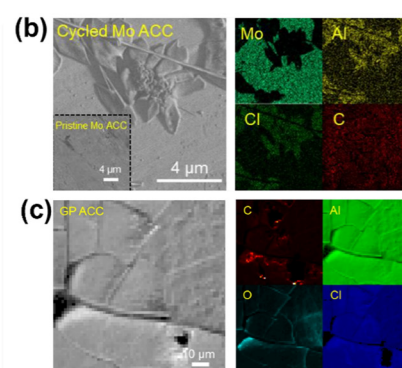


Fig. 10 Electrochemical measurements and *ex situ* characterization of different anodic CCs. (a) Cycling performance of different anodic CCs at a fixed rate of  $50 \text{ mA g}^{-1}$  (b) SEM and EDX measurements of fully discharged Mo anodic CC after 100 cycles. (c) AES image and corresponding AES elemental mapping of fully charged GP anodic CC etched for 20 min by argon ion bombardment. Reprinted with permission,<sup>128</sup> Elsevier, Copyright 2022.



**Table 5** Summary of composition and electrochemical properties for the different AFAMBs. VW = voltage window, SC = specific capacity, CR = capacity retention

CC	Electrolyte	Cathode	VW/V	SC/mA h g <sup>-1</sup>	CR/cycles	Current Density	Ref.
Al	AlCl <sub>3</sub> /[EMIm]Cl	Graphite Paper	1.5–2.5	58	98.6%/1000	0.2 A g <sup>-1</sup>	128
GP	AlCl <sub>3</sub> /[EMIm]Cl	Graphite Paper	1.5–2.5	54.6	98.1%/1000	0.2 A g <sup>-1</sup>	128
Mo	AlCl <sub>3</sub> /[EMIm]Cl	Graphite Paper	1.5–2.5	53.2	95.8%/1000	0.2 A g <sup>-1</sup>	128
Ag	AlCl <sub>3</sub> /[EMIm]Cl	Graphite Paper	1.5–2.5	~28	0%/300	0.2 A g <sup>-1</sup>	128
Ni	AlCl <sub>3</sub> /[EMIm]Cl	Graphite Paper	1.5–2.5	~25	0%/~150	0.2 A g <sup>-1</sup>	128
SS304	AlCl <sub>3</sub> /[EMIm]Cl	Graphite Paper	1.5–2.5	~20	0%/~670	0.2 A g <sup>-1</sup>	128
Mg	AlCl <sub>3</sub> /[EMIm]Cl	Graphite Paper	1.5–2.5	~10	0%/~400	0.2 A g <sup>-1</sup>	128
Cu	AlCl <sub>3</sub> /[EMIm]Cl	Graphite Paper	1.5–2.5	~35	0%/~140	0.2 A g <sup>-1</sup>	128
Au-SS	Aqueous/ZnBr <sub>2</sub> , TPABr	Graphene	1.5–2.5	~45	74%/2000	1.4 mA cm <sup>-2</sup>	127
Au@Ti	Aqueous/ZnSO <sub>4</sub> Zn(OTF) <sub>2</sub>	EG	0.5–2.3	107.4	80%/900	0.2 A g <sup>-1</sup>	131

homogeneity of the plating and thus on the growth of dendrites. They hypothesize that a lattice mismatch between CC and Al below 15% is necessary for the electrochemical plating of dense Al layers. Their calculations have shown that the (111) facet of Al has the lowest surface energy (0.96 J m<sup>-2</sup>), which favors compact growth in this orientation. To take advantage of these properties, they investigated the Al plating/stripping behavior of SS CCs coated with a 2D Au structure that predominantly exposes the (111) crystal plane. Au has a lattice mismatch of only about 0.72% compared to Al, which significantly improves the plating homogeneity compared to uncoated CCs. The nucleation density of particles is drastically increased with an average size below 250 nm, whereas on the SS, which has a large lattice mismatch, clusters, and dendritic structures dominate. In a cell configuration of SS-Au/Au-Al, Zhao *et al.* achieved plating/stripping efficiencies of over 99% for 500 cycles. This is especially good considering that the CC was made of SS, which can be corroded by the electrolyte.<sup>128</sup>

Meng *et al.* improved this concept by using titanium (Ti) as the CC with a 10 nm Au lattice-matching layer, resulting in an average CE of 99.92% for more than 4500 h in a cell *versus* Al-Metal.<sup>131</sup> In a dual-ion battery configuration with Ti/Au as an anode and graphite as the cathode, a CE > 98% was achieved with a capacity retention of more than 78% after 2000 cycles. Furthermore, a reduction of the Au layer thickness to 2 nm did not significantly decrease the stability of the plating/stripping.

### 9.3. Summary of AFAMB development

The discussion above emphasizes the importance of the crystal structure, interfacial structures, and nucleation sites for anode-free AIBs. However, in terms of a commercial application, it can be argued that the anode-free approach for the case of Al-ion batteries is only suitable for niche applications. The low effort of using Al-metal as an anode and CC at the same time and the low price and abundance of the metal make the usage of more complex approaches using surface modification and less abundant materials unattractive.<sup>132</sup> This is especially true since the main advantage of Al is supposed to be the low price and abundance. For an anode-free approach to be feasible, a stable cathode of the conversion type or one that intercalates Al cations has to be discovered.<sup>133</sup> Additionally, it has to be manufactured in a fully charged state. Since the only good performing and stable Al-ion batteries are based on carbon

cathodes and nonaqueous chloroaluminate-based ionic liquids as electrolytes and therefore the intercalation of chloroaluminate anions, they are dual ion batteries and the amount of electrolyte can be a limiting factor for the achievable capacity.<sup>127</sup> The high price of non-aqueous chloroaluminate-based electrolytes and the amount needed is prohibitive for a successful commercialization. The composition and electrochemical properties for the different AFAMBs are summarized in Table 5.

## 10. Conclusions and perspectives

In the present article, recent developments in anode-free metal batteries that offer an alternative to anode-free lithium batteries are reviewed. The metals considered were Na, K, Mg, Zn, and Al. Seeking a common denominator to the understanding of the present problem in a unified framework, special fundamentals to the concept of metal-philicity are provided, which denominates the affinity of a metal for being deposited on the CC, relative to the affinity of the metal for itself. This idea seems to be common to all the systems studied and plays a very important role in reducing the nucleation overpotential for metal plating, in producing a smooth deposit, and in preventing the formation of dendrites. Since this concept is often expressed quantitatively in terms of the binding energy of a metal atom to a surface, which is assessed by DFT first-principles calculations, a whole section is devoted to the computational studies of AFMBs. The performance of AFMBs could only be improved if the nucleation and growth mechanisms of the corresponding metals and the electrolyte decomposition, SEI and dead-metal formation on the corresponding metals are well-explored.

Promising electrochemical performances have been obtained in full-cell configurations, but in all cases the CE and specific capacity are still decreasing during cycling. In this sense, the modification and coating of the CC surface, which induces the desired metal philicity, plays a fundamental role in the ordered plating of the metals, diminishing the overpotentials and the dendrite formation. There are some common materials for AFMBs, such as M-Xenes, carbon coatings, metal alloys, nanoparticles, *etc.*, which could allow the consideration of these strategies as a possible general solution for the different AFMBs.

All these coatings have in common that they exhibit a high surface energy compared to the surface energy of the metal to be deposited. A high surface energy is generally achieved by introducing a functionalization with a high defect density, *e.g.* Nitrogen defects, vacancies or polar -F or -NH sites.

Furthermore, a functionalization of the separator side facing the metal can be beneficial. As for the CC, a good wettability between separator and metal enable a homogeneous nucleation which is especially important for anode free batteries. To ensure a planar growth of the metal, the electrolyte should be tuned such, that a smooth and strong anion-derived SEI can build up. Ideally, such a strong SEI that does not break during cycling can guide the metal to grow as a planar film. One further requirement for the SEI is that its ion channels have to be evenly distributed. As is well known by now, a SEI is rarely comprised of one single compound but rather agglomerates of different decomposition products, which can have totally different ionic conductivities. Therefore, an even distribution is necessary to avoid uneven electroplating and thereby continuous rupture and reformation of the SEI.

### Broader implications and future directions

- More research is needed in the field of an artificial SEI or in the case of an anode-free battery of a functionalized separator. Here, the interaction energy between the SEI and the metal to be deposited should be low, so that the SEI does not get destroyed by the volumetric changes of the metal anode.

- The authors suggest to enable a homogenous metal nucleation by an adjustment of the cycling routine. A pulsed deposition in the first formation cycle can result in a much more homogeneous plating. In this context, the series resistance of all individual components should be taken into focus of research as the network of all series resistances is what determines the electric field distribution.

- The study of Fang and al.<sup>134</sup> indicates that also the cell pressure affects the homogeneity of the plated metal morphology, *i.e.* a high cell pressure promotes planar growth. However, this parameter is not yet in the focus of AFMB-research. Therefore, for future works the authors suggest to provide detailed information about the stacking height and the spring chosen for coin cells. Advanced *in situ* imaging techniques such as *in situ* optical microscopy, transmission X-ray microscopy, and similar need to be further developed to learn more about the nucleation and growth mechanisms of different metals. Meanwhile, *in situ* spectroscopic techniques such as *in situ* FTIR, *in situ* Raman, *in situ* XPS, *in situ* NMR etc. should be used to explore the electrolyte decomposition, SEI and dead-metal formation on various metals.

- More studies on binding energies between the individual battery components - CC, metal anode, SEI and separator - will help to effectively tackle the main difficulties.

- Recycling and life-cycle analysis: It's crucial to assess the recyclability and overall environmental impact of AFMBs throughout their lifecycle to ensure they truly represent a sustainable alternative.

- Scalability: While lab-scale demonstrations are encouraging, the scalability of AFMB production processes needs careful evaluation to meet the demands of large-scale energy storage – especially with respect to safety concerns during fabrication and operation.

Overall: post-lithium AFMBs seek to improve cost-effectiveness through the use of abundant and inexpensive materials, streamlined manufacturing processes, and an increased energy density, making energy storage more accessible and economically viable. These advances have the potential to drive innovation in various industries, leading to more sustainable, efficient, and affordable energy in the future.

### Author contributions

Deik Petersen, Monja Gronenberg, German Lener, Sasan Rostami: writing – original draft, investigation, methodology, validation, writing – review & editing. Ezequiel P.M. Leiva, Guillermina L. Luque: writing – original draft, investigation, methodology, writing – review & editing, funding acquisition, project administration. Andrea Paoella: investigation, writing – review & editing. Bing Joe Hwang: writing – review & editing. Rainer Adelung: writing – review & editing, funding acquisition, project administration. Mozaffar Abdollahifar: writing – original draft, investigation, validation, methodology, writing – review & editing, supervision, project administration.

### Data availability

All data discussed in this review paper can be found in the original papers (references).

### Conflicts of interest

The authors declare no conflict of interest.

### Acknowledgements

D. P. and M. G. contributed equally to this work. This work was supported by the financial support of the German Federal Ministry for Education and Research (BMBF) for the funding of the research project of SiLiNE (Reference No. 03XP0419B), and also the project "SuSiBaby" – SulfurSilicon Batteries (LPWE/3.1.1/1801) funded by the EUSH and the European Regional Development Fund of the European Union in Schleswig-Holstein, Germany, and the project "Medesteer" (NSTC 112-2639- E-011-001-ASP) funded by the National Science and Technology Council, Taiwan. E. P. M. L. acknowledges grants PIP CONICET 1220200101189CO, PUE/2017 CONICET, FONCYT 2020-SERIEA-03689.

### References

- Z. P. Cano, D. Banham, S. Ye, A. Hintennach, J. Lu, M. Fowler and Z. Chen, Batteries and fuel cells for emerging electric vehicle markets, *Nat. Energy*, 2018, 3, 279–289.



2 F. Degen, M. Winter, D. Bendig and J. Tübke, Energy consumption of current and future production of lithium-ion and post lithium-ion battery cells, *Nat. Energy*, 2023, **8**, 1284–1295.

3 D. Larcher and J.-M. Tarascon, Towards greener and more sustainable batteries for electrical energy storage, *Nat. Chem.*, 2015, **7**, 19–29.

4 A. Rahman, O. Farrok and M. M. Haque, Environmental impact of renewable energy source based electrical power plants: Solar, wind, hydroelectric, biomass, geothermal, tidal, ocean, and osmotic, *Renewable Sustainable Energy Rev.*, 2022, **161**, 112279.

5 S. Chu, Y. Cui and N. Liu, The path towards sustainable energy, *Nat. Mater.*, 2017, **16**, 16–22.

6 H. Cavers, P. Molaiyan, M. Abdollahifar, U. Lassi and A. Kwade, Perspectives on Improving the Safety and Sustainability of High Voltage Lithium-Ion Batteries Through the Electrolyte and Separator Region, *Adv. Energy Mater.*, 2022, **12**, 2200147.

7 N. Sick, O. Krätzig, G. G. Eshetu and E. Figgemeier, A review of the publication and patent landscape of anode materials for lithium ion batteries, *J. Energy Storage*, 2021, **43**, 103231.

8 [Cannot display the reference "", because the template "Bibliography - Book - (Default template)" contains only fields that are empty in this reference.].

9 K. B. Hatzell, Anode-Less or Anode-Free?, *ACS Energy Lett.*, 2023, **8**, 4775–4776.

10 S. Chen, Y. Xia, R. Zeng, Z. Luo, X. Wu, X. Hu, J. Lu, E. Gazit, H. Pan and Z. Hong, Ordered planar plating/stripping enables deep cycling zinc metal batteries, *Sci. Adv.*, 2024, **10**, eadn2265.

11 H. Liu, X.-B. Cheng, R. Xu, X.-Q. Zhang, C. Yan, J.-Q. Huang and Q. Zhang, Plating/stripping behavior of actual lithium metal anode, *Adv. Energy Mater.*, 2019, **9**, 1902254.

12 S.-H. Wang, Y.-X. Yin, T.-T. Zuo, W. Dong, J.-Y. Li, J.-L. Shi, C.-H. Zhang, N.-W. Li, C.-J. Li and Y.-G. Guo, Stable Li metal anodes via regulating lithium plating/stripping in vertically aligned microchannels, *Adv. Mater.*, 2017, **29**, 1703729.

13 L. Hu, J. Deng, Y. Lin, Q. Liang, B. Ge, Q. Weng, Y. Bai, Y. Li, Y. Deng and G. Chen, Restructuring Electrolyte Solvation by a Versatile Diluent Toward Beyond 99.9% Coulombic Efficiency of Sodium Plating/Stripping at Ultralow Temperatures, *Adv. Mater.*, 2024, 2312161.

14 X. Duan, B. Li, J. Li, X. Gao, L. Wang and J. Xu, Quantitative Understanding of Lithium Deposition-Stripping Process on Graphite Anodes of Lithium-Ion Batteries, *Adv. Energy Mater.*, 2023, **13**, 2203767.

15 M. Wang, X. Zheng, X. Zhang, D. Chao, S.-Z. Qiao, H. N. Alshareef, Y. Cui and W. Chen, Opportunities of aqueous manganese-based batteries with deposition and stripping chemistry, *Adv. Energy Mater.*, 2021, **11**, 2002904.

16 S. Ferrari, M. Falco, A. B. Muñoz-García, M. Bonomo, S. Brutt, M. Pavone and C. Gerbaldi, Solid-state post Li metal ion batteries: a sustainable forthcoming reality?, *Adv. Energy Mater.*, 2021, **11**, 2100785.

17 D. Jin, J. Park, M.-H. Ryou and Y. M. Lee, Structure-controlled Li metal electrodes for post-Li-ion batteries: recent progress and perspectives, *Adv. Mater. Interfaces*, 2020, **7**, 1902113.

18 P. Liu and D. Mitlin, Emerging potassium metal anodes: perspectives on control of the electrochemical interfaces, *Acc. Chem. Res.*, 2020, **53**, 1161–1175.

19 M. Tang, S. Dong, J. Wang, L. Cheng, Q. Zhu, Y. Li, X. Yang, L. Guo and H. Wang, Low-temperature anode-free potassium metal batteries, *Nat. Commun.*, 2023, **14**, 6006.

20 Y. Zhao, K. R. Adair and X. Sun, Recent developments and insights into the understanding of Na metal anodes for Na-metal batteries, *Energy Environ. Sci.*, 2018, **11**, 2673–2695.

21 Y. Liu, Y. Li, J. Sun, Z. Du, X. Hu, J. Bi, C. Liu, W. Ai and Q. Yan, Present and future of functionalized Cu current collectors for stabilizing lithium metal anodes, *Nano Research Energy*, 2023, **2**, e9120048.

22 P. Molaiyan, M. Abdollahifar, B. Boz, A. Beutl, M. Krammer, N. Zhang, A. Tron, M. Romio, M. Ricci, R. Adelung, A. Kwade, U. Lassi and A. Paoletta, Optimizing Current Collector Interfaces for Efficient "Anode-Free" Lithium Metal Batteries, *Adv. Funct. Mater.*, 2023, 2311301.

23 Y. Fei, J. Jiang, L. Zhang, P. Nie, Y. Jiang, Y. Chen, Q. Zhuang and Z. Ju, Potassophilic  $\alpha$ -MoC anchored on 3D carbon host enables uniform potassium nucleation and super-stable potassium metal anodes, *Chem. Eng. J.*, 2024, **490**, 151527.

24 S. Li, H. Zhu, Y. Liu, Z. Han, L. Peng, S. Li, C. Yu, S. Cheng and J. Xie, Codoped porous carbon nanofibres as a potassium metal host for nonaqueous K-ion batteries, *Nat. Commun.*, 2022, **13**, 4911.

25 Z. Li, L. Ma, K. Han, Y. Ji, J. Xie, L. Pan, J. Li and W. Mai, A host potassophilicity strategy for unprecedentedly stable and safe K metal batteries, *Chem. Sci.*, 2023, **14**, 9114–9122.

26 V. Pande and V. Viswanathan, Computational Screening of Current Collectors for Enabling Anode-Free Lithium Metal Batteries, *ACS Energy Lett.*, 2019, **4**, 2952–2959.

27 Y. Wang, J. Tan, Z. Li, L. Ma, Z. Liu, M. Ye and J. Shen, Recent progress on enhancing the Lithiophilicity of hosts for dendrite-free lithium metal batteries, *Energy Storage Mater.*, 2022, **53**, 156–182.

28 Q. Bai, L. Yang, H. Chen and Y. Mo, Computational Studies of Electrode Materials in Sodium-Ion Batteries, *Adv. Energy Mater.*, 2018, **8**, 1702998.

29 A. M. Nolan, Y. Zhu, X. He, Q. Bai and Y. Mo, Computation-Accelerated Design of Materials and Interfaces for All-Solid-State Lithium-Ion Batteries, *Joule*, 2018, **2**, 2016–2046.

30 X. Chen, T. Hou, K. A. Persson and Q. Zhang, Combining theory and experiment in lithium–sulfur batteries: Current progress and future perspectives, *Mater. Today*, 2019, **22**, 142–158.

31 E. Paquet and H. L. Viktor, Computational Methods for Ab Initio Molecular Dynamics, *Adv. Chem.*, 2018, **2018**, 1–14.

32 X. Chen, X.-R. Chen, T.-Z. Hou, B.-Q. Li, X.-B. Cheng, R. Zhang and Q. Zhang, Lithiophilicity chemistry of

heteroatom-doped carbon to guide uniform lithium nucleation in lithium metal anodes, *Sci. Adv.*, 2019, **5**, eaau7728.

33 K. Yan, Z. Lu, H.-W. Lee, F. Xiong, P.-C. Hsu, Y. Li, J. Zhao, S. Chu and Y. Cui, Selective deposition and stable encapsulation of lithium through heterogeneous seeded growth, *Nat. Energy*, 2016, **1**, 1–8.

34 Y. Wang, Y. Liu, M. Nguyen, J. Cho, N. Katyal, B. S. Vishnugopi, H. Hao, R. Fang, N. Wu, P. Liu, P. P. Mukherjee, J. Nanda, G. Henkelman, J. Watt and D. Mitlin, Stable Anode-Free All-Solid-State Lithium Battery through Tuned Metal Wetting on the Copper Current Collector, *Adv. Mater.*, 2023, **35**, e2206762.

35 W. Shin and A. Manthiram, Fast and Simple Ag/Cu Ion Exchange on Cu Foil for Anode-Free Lithium-Metal Batteries, *ACS Appl. Mater. Interfaces*, 2022, **14**, 17454–17460.

36 S. Cho, D. Y. Kim, J.-I. Lee, J. Kang, H. Lee, G. Kim, D.-H. Seo and S. Park, Highly Reversible Lithium Host Materials for High-Energy-Density Anode-Free Lithium Metal Batteries, *Adv. Funct. Mater.*, 2022, **32**, 2208629.

37 X. Chen, Y.-K. Bai, X. Shen, H.-J. Peng and Q. Zhang, Sodiophilicity/potassiophilicity chemistry in sodium/potassium metal anodes, *J. Energy Chem.*, 2020, **51**, 1–6.

38 Q. Ni, Y. Yang, H. Du, H. Deng, J. Lin, L. Lin, M. Yuan, Z. Sun and G. Sun, Anode-Free Rechargeable Sodium-Metal Batteries, *Batteries*, 2022, **8**, 272.

39 L. Zhang, Y. Xia, H. Yang, S. Xiao, J. Zhou, Y. Cao and T. Qian, The current status of sodium metal anodes for improved sodium batteries and its future perspectives, *APL Mater.*, 2022, **10**, 070901.

40 Q. Lu, A. Yang, A. Omar, Q. Ma, F. Tietz, O. Guillon and D. Mikhailova, Recent Advances in Stabilization of Sodium Metal Anode in Contact with Organic Liquid and Solid-State Electrolytes, *Energy Technol.*, 2022, **10**, 2200149.

41 J. Xu, J. Yang, Y. Qiu, Y. Jin, T. Wang, B. Sun and G. Wang, Achieving high-performance sodium metal anodes: From structural design to reaction kinetic improvement, *Nano Res.*, 2023, 1–25.

42 S. Nanda, A. Gupta and A. Manthiram, Anode-Free Full Cells: A Pathway to High-Energy Density Lithium-Metal Batteries, *Adv. Energy Mater.*, 2021, **11**, 2000804.

43 T. Yang, D. Luo, Y. Liu, A. Yu and Z. Chen, Anode-free sodium metal batteries as rising stars for lithium-ion alternatives, *iScience*, 2023, **26**, 105982.

44 Z. Hu, L. Liu, X. Wang, Q. Zheng, C. Han and W. Li, Current Progress of Anode-Free Rechargeable Sodium Metal Batteries: Origin, Challenges, Strategies, and Perspectives, *Adv. Funct. Mater.*, 2024, **34**, 2313823.

45 T. Yang, D. Luo, Y. Liu, A. Yu and Z. Chen, Anode-free sodium metal batteries as rising stars for lithium-ion alternatives, *iScience*, 2023, **26**, 105982.

46 Y. Chen, C. Ye, N. Zhang, J. Liu, H. Li, K. Davey and S.-Z. Qiao, Prospects for practical anode-free sodium batteries, *Mater. Today*, 2024, **73**, 260–274.

47 X. Cheng, D. Li, S. Peng, P. Shi, H. Yu, Y. Jiang and S. Li, *in situ* Alloy-Modified Sodiophilic Current Collectors for Anode-Less Sodium Metal Batteries, *Batteries*, 2023, **9**, 408.

48 K. Lee, Y. J. Lee, M. J. Lee, J. Han, J. Lim, K. Ryu, H. Yoon, B.-H. Kim, B. J. Kim and S. W. Lee, A 3D Hierarchical Host with Enhanced Sodiophilicity Enabling Anode-Free Sodium-Metal Batteries, *Adv. Mater.*, 2022, **34**, e2109767.

49 T.-S. Wang, Y. Liu, Y.-X. Lu, Y.-S. Hu and L.-Z. Fan, Dendrite-free Na metal plating/stripping onto 3D porous Cu hosts, *Energy Storage Mater.*, 2018, **15**, 274–281.

50 C. Wang, Y. Zheng, Z.-N. Chen, R. Zhang, W. He, K. Li, S. Yan, J. Cui, X. Fang, J. Yan, G. Xu, D. Peng, B. Ren and N. Zheng, Robust Anode-Free Sodium Metal Batteries Enabled by Artificial Sodium Formate Interface, *Adv. Energy Mater.*, 2023, **13**, 2204125.

51 H. Li, H. Zhang, F. Wu, M. Zarrabeitia, D. Geiger, U. Kaiser, A. Varzi and S. Passerini, Sodiophilic Current Collectors Based on MOF-Derived Nanocomposites for Anode-Less Na-Metal Batteries, *Adv. Energy Mater.*, 2022, **12**, 2202293.

52 Y. Lu, Q. Zhang, M. Han and J. Chen, Stable Na plating/stripping electrochemistry realized by a 3D Cu current collector with thin nanowires, *Chem. Commun.*, 2017, **53**, 12910–12913.

53 A. P. Cohn, N. Muralidharan, R. Carter, K. Share and C. L. Pint, Anode-Free Sodium Battery through in Situ Plating of Sodium Metal, *Nano Lett.*, 2017, **17**, 1296–1301.

54 O. J. Dahunsi, B. Li, B. An, I. B. Abdul Razak, F. Xia, S. Gao, J. Chen, G. Li and Y. Cheng, Directing High-Efficiency Na Plating with Carbon-Aluminum Junction Interfaces for Anode-Free Na Metal Batteries, *Energy Fuels*, 2023, **37**, 7522–7529.

55 A. P. Cohn, T. Metke, J. Donohue, N. Muralidharan, K. Share and C. L. Pint, Rethinking sodium-ion anodes as nucleation layers for anode-free batteries, *J. Mater. Chem. A*, 2018, **6**, 23875–23884.

56 M. E. Lee, S. Lee, J. Choi, H.-J. Jin, S. Han and Y. S. Yun, Anode-Free Sodium Metal Batteries Based on Nanohybrid Core-Shell Templates, *Small*, 2019, **15**, e1901274.

57 H. Wang, Y. Wu, S. Liu, Y. Jiang, D. Shen, T. Kang, Z. Tong, D. Wu, X. Li and C.-S. Lee, 3D Ag@C Cloth for Stable Anode Free Sodium Metal Batteries, *Small Methods*, 2021, **5**, e2001050.

58 P. Liu, H. Yi, S. Zheng, Z. Li, K. Zhu, Z. Sun, T. Jin and L. Jiao, Regulating Deposition Behavior of Sodium Ions for Dendrite-Free Sodium-Metal Anode, *Adv. Energy Mater.*, 2021, **11**, 2101976.

59 W. Bai, Y. Wang, T. Xu, D. Kong, S. Zhang, X. Wang, X. Li, H. Wang and Y. Jiang, Sodiophilic three-dimensional carbon skeleton derived from polyacrylonitrile@zeolitic imidazolate framework fiber for dendrite-free sodium metal anode, *J. Power Sources*, 2022, **551**, 232165.

60 L. Wang, N. Ren, Y. Yao, H. Yang, W. Jiang, Z. He, Y. Jiang, S. Jiao, L. Song, X. Wu, Z.-S. Wu and Y. Yu, Designing Solid Electrolyte Interfaces towards Homogeneous Na Deposition: Theoretical Guidelines for Electrolyte Additives and Superior High-Rate Cycling Stability, *Angew. Chem., Int. Ed.*, 2023, **62**, e202214372.

61 Y. Wang, H. Dong, N. Katyal, H. Hao, P. Liu, H. Celio, G. Henkelman, J. Watt and D. Mitlin, A Sodium-Antimony-Telluride Intermetallic Allows Sodium-Metal Cycling at

100% Depth of Discharge and as an Anode-Free Metal Battery, *Adv. Mater.*, 2022, **34**, e2106005.

62 W. Zhang, J. Yin, W. Wang, Z. Bayhan and H. N. Alshareef, Status of rechargeable potassium batteries, *Nano Energy*, 2021, **83**, 105792.

63 C. Wei, Y. Tao, H. Fei, Y. An, Y. Tian, J. Feng and Y. Qian, Recent advances and perspectives in stable and dendrite-free potassium metal anodes, *Energy Storage Mater.*, 2020, **30**, 206–227.

64 S. Li, H. Zhu, C. Gu, F. Ma, W. Zhong, M. Liu, H. Zhang, Z. Zeng, S. Cheng and J. Xie, Customized Electrolyte and Host Structures Enabling High-Energy-Density Anode-Free Potassium–Metal Batteries, *ACS Energy Lett.*, 2023, **8**, 3467–3475.

65 J. Meng, H. Zhu, Z. Xiao, X. Zhang, C. Niu, Y. Liu, G. Jiang, X. Wang, F. Qiao, X. Hong, F. Liu, Q. Pang and L. Mai, Amine-Wetting-Enabled Dendrite-Free Potassium Metal Anode, *ACS Nano*, 2022, **16**, 7291–7300.

66 J. Wang, Y. Zuo, M. Chen, K. Chen, Z. Chen, Z. Lu and L. Si, Bifunctional separator with a light-weight coating for stable anode-free potassium metal batteries, *Electrochim. Acta*, 2022, **433**, 141211.

67 L. Si, J. Wang, M. Chen, K. Chen, Z. Chen, Z. Lu, Y. Zhang, Y. Zhang and H. Liu, Stable Solid Electrolyte Interface Achieved by Separator Surface Modification for High-Performance Anode-free Potassium Metal Batteries, *ACS Appl. Energy Mater.*, 2023, **6**, 326–333.

68 M. Tang, S. Dong, J. Wang, L. Cheng, Q. Zhu, Y. Li, X. Yang, L. Guo and H. Wang, Low-temperature anode-free potassium metal batteries, *Nat. Commun.*, 2023, **14**, 6006.

69 P. Liu, Y. Wang, Q. Gu, J. Nanda, J. Watt and D. Mitlin, Dendrite-Free Potassium Metal Anodes in a Carbonate Electrolyte, *Adv. Mater.*, 2020, **32**, 1906735.

70 Y. Li, L. Zhang, S. Liu, X. Wang, D. Xie, X. Xia, C. Gu and J. Tu, Original growth mechanism for ultra-stable dendrite-free potassium metal electrode, *Nano Energy*, 2019, **62**, 367–375.

71 Y. Zhao, B. Liu, Y. Yi, X. Lian, M. Wang, S. Li, X. Yang and J. Sun, An Anode-Free Potassium-Metal Battery Enabled by a Directly Grown Graphene-Modulated Aluminum Current Collector, *Adv. Mater.*, 2022, **34**, 2202902.

72 X. Tang, D. Zhou, P. Li, X. Guo, B. Sun, H. Liu, K. Yan, Y. Gogotsi and G. Wang, MXene-Based Dendrite-Free Potassium Metal Batteries, *Adv. Mater.*, 2020, **32**, 1906739.

73 J. Wang, W. Yan and J. Zhang, High area capacity and dendrite-free anode constructed by highly potassophilic Pd/Cu current collector for low-temperature potassium metal battery, *Nano Energy*, 2022, **96**, 107131.

74 N. Xiao, W. D. McCulloch and Y. Wu, Reversible Dendrite-Free Potassium Plating and Stripping Electrochemistry for Potassium Secondary Batteries, *J. Am. Chem. Soc.*, 2017, **139**, 9475–9478.

75 L. Xue, Y. Li, H. Gao, W. Zhou, X. Lü, W. Kaveevivitchai, A. Manthiram and J. B. Goodenough, Low-Cost High-Energy Potassium Cathode, *J. Am. Chem. Soc.*, 2017, **139**, 2164–2167.

76 C. Wei, L. Tan, Y. Zhang, Z. Wang, J. Feng and Y. Qian, Towards better Mg metal anodes in rechargeable Mg batteries: Challenges, strategies, and perspectives, *Energy Storage Mater.*, 2022, **52**, 299–319.

77 C. Heubner, S. Maletti, H. Auer, J. Hüttl, K. Voigt, O. Lohrberg, K. Nikolowski, M. Partsch and A. Michaelis, From Lithium-Metal toward Anode-Free Solid-State Batteries: Current Developments, Issues, and Challenges, *Adv. Funct. Mater.*, 2021, **31**, 2106608.

78 C. Ling, D. Banerjee and M. Matsui, Study of the electrochemical deposition of Mg in the atomic level: Why it prefers the non-dendritic morphology, *Electrochim. Acta*, 2012, **76**, 270–274.

79 M. Jäckle and A. Groß, Microscopic properties of lithium, sodium, and magnesium battery anode materials related to possible dendrite growth, *J. Chem. Phys.*, 2014, **141**, 174710.

80 J. H. Kwak, Y. Jeoun, S. H. Oh, S. Yu, J.-H. Lim, Y.-E. Sung, S.-H. Yu and H.-D. Lim, Operando Visualization of Morphological Evolution in Mg Metal Anode: Insight into Dendrite Suppression for Stable Mg Metal Batteries, *ACS Energy Lett.*, 2022, **7**, 162–170.

81 M. Mao, X. Fan, W. Xie, H. Wang, L. Suo and C. Wang, The Proof-of-Concept of Anode-Free Rechargeable Mg Batteries, *Adv. Sci.*, 2023, **10**, e2207563.

82 Y.-J. Chang, Y.-S. Huang and P.-W. Chu, Microstructure and the Plating/Stripping Behavior of Magnesium Metal Negative Electrode for Rechargeable Magnesium Batteries, *Meet. Abstr.*, 2023, **01**, 413.

83 J. Bae, H. Park, X. Guo, X. Zhang, J. H. Warner and G. Yu, High-performance magnesium metal batteries via switching the passivation film into a solid electrolyte interphase, *Energy Environ. Sci.*, 2021, **14**, 4391–4399.

84 J. Liu, M. Wang, Z. Zhang, J. Zhang, Y. He, Z. Zhou and G. Li, Unlock the full potential of carbon cloth-based scaffolds towards magnesium metal storage via regulation on magnesiophilicity and surface geometric structure, *J. Energy Chem.*, 2024, **90**, 423–434.

85 J. Song, J. Chen, X. Xiong, X. Peng, D. Chen and F. Pan, Research advances of magnesium and magnesium alloys worldwide in 2021, *Journal of Magnesium and Alloys*, 2022, **10**, 863–898.

86 S. S. Shinde, N. K. Wagh, S.-H. Kim and J.-H. Lee, Li, Na, K, Mg, Zn, Al, and Ca Anode Interface Chemistries Developed by Solid-State Electrolytes, *Adv. Sci.*, 2023, **10**, e2304235.

87 Y. Li, X. Feng, W. Y. Lieu, L. Fu, C. Zhang, T. Ghosh, A. Thakur, B. C. Wyatt, B. Anasori, W. Liu, Q. Zhang, J. Lu and Z. W. Seh, MXene-Based Anode-Free Magnesium Metal Battery, *Adv. Funct. Mater.*, 2023, **33**, 2303067.

88 Y. Li, G. Yang, S. Sun, C. Zhang, C. Y. J. Lim, A. J. Y. Wong, W. Y. Lieu, Z. Sofer, M.-F. Ng, W. Liu and Z. W. Seh, High Utilization of Composite Magnesium Metal Anodes Enabled by a Magnesiophilic Coating, *Nano Lett.*, 2022, **22**, 6808–6815.

89 G. Yang, Y. Li, C. Zhang, J. Wang, Y. Bai, C. Y. J. Lim, M.-F. Ng, Z. Chang, S. Kumar, Z. Sofer, W. Liu and Z. W. Seh,

In Situ Formed Magnesiophilic Sites Guiding Uniform Deposition for Stable Magnesium Metal Anodes, *Nano Lett.*, 2022, **22**, 9138–9146.

90 Y. Wang, F. Cheng, Y. Huang, C. Cai and Y. Fu, Vertically-oriented growth of MgMOF layer via heteroepitaxial guidance for highly stable magnesium-metal anode, *Energy Storage Mater.*, 2023, **61**, 102911.

91 H.-D. Lim, D. H. Kim, S. Park, M. E. Lee, H.-J. Jin, S. Yu, S. H. Oh and Y. S. Yun, Magnesiophilic Graphitic Carbon Nanosubstrate for Highly Efficient and Fast-Rechargeable Mg Metal Batteries, *ACS Appl. Mater. Interfaces*, 2019, **11**, 38754–38761.

92 J. Liu, J. Zhang, Z. Zhang, A. Du, S. Dong, Z. Zhou, X. Guo, Q. Wang, Z. Li, G. Li and G. Cui, Epitaxial Electrocristallization of Magnesium via Synergy of Magnesiophilic Interface, Lattice Matching, and Electrostatic Confinement, *ACS Nano*, 2022, **16**, 9894–9907.

93 J. H. Kwak, S. Shin, Y. Jeoun, Y. Lee, S. Yu, Y. S. Yun, Y.-E. Sung, S.-H. Yu and H.-D. Lim, Facile synthesis of three-dimensional conducting scaffold with magnesiophilic decorations toward non-dendritic Mg-metal batteries, *J. Power Sources*, 2022, **541**, 231724.

94 Z. Song, Z. Zhang, A. Du, S. Dong, G. Li and G. Cui, Uniform Magnesium Electrodeposition via Synergistic Coupling of Current Homogenization, Geometric Confinement, and Chemisorption Effect, *Adv. Mater.*, 2021, **33**, e2100224.

95 J. H. Kwak, S. Park, S. Shin, S. Park, C. Kang, S.-H. Yu, J. Moon and H.-D. Lim, Geometrical design of top-to-bottom magnesiophilicity-gradient host for reversible Mg-metal batteries, *Energy Storage Mater.*, 2023, **59**, 102762.

96 O. Mizrahi, N. Amir, E. Pollak, O. Chusid, V. Marks, H. Gottlieb, L. Larush, E. Zinigrad and D. Aurbach, Electrolyte Solutions with a Wide Electrochemical Window for Rechargeable Magnesium Batteries, *J. Electrochem. Soc.*, 2008, **155**, A103.

97 R. Deivanayagam, B. J. Ingram and R. Shahbazian-Yassar, Progress in development of electrolytes for magnesium batteries, *Energy Storage Mater.*, 2019, **21**, 136–153.

98 I. Shterenberg, M. Salama, Y. Gofer and D. Aurbach, Hexafluorophosphate-Based Solutions for Mg Batteries and the Importance of Chlorides, *Langmuir*, 2017, **33**, 9472–9478.

99 Z. Ma, D. R. MacFarlane and M. Kar, Mg Cathode Materials and Electrolytes for Rechargeable Mg Batteries: A Review, *Batteries Supercaps*, 2019, **2**, 115–127.

100 R. Attias, M. Salama, B. Hirsch, Y. Goffer and D. Aurbach, Anode-Electrolyte Interfaces in Secondary Magnesium Batteries, *Joule*, 2019, **3**, 27–52.

101 Y. Sun, F. Ai and Y.-C. Lu, Electrolyte and Interphase Design for Magnesium Anode: Major Challenges and Perspectives, *Small*, 2022, **18**, e2200009.

102 D. Aurbach, Z. Lu, A. Schechter, Y. Gofer, H. Gizbar, R. Turgeman, Y. Cohen, M. Moshkovich and E. Levi, Prototype systems for rechargeable magnesium batteries, *Nature*, 2000, **407**, 724–727.

103 M. M. Huie, D. C. Bock, E. S. Takeuchi, A. C. Marschilok and K. J. Takeuchi, Cathode materials for magnesium and magnesium-ion based batteries, *Coord. Chem. Rev.*, 2015, **287**, 15–27.

104 N. Pour, Y. Gofer, D. T. Major and D. Aurbach, Structural analysis of electrolyte solutions for rechargeable Mg batteries by stereoscopic means and DFT calculations, *J. Am. Chem. Soc.*, 2011, **133**, 6270–6278.

105 D.-T. Nguyen, A. Y. S. Eng, M.-F. Ng, V. Kumar, Z. Sofer, A. D. Handoko, G. S. Subramanian and Z. W. Seh, A High-Performance Magnesium Triflate-based Electrolyte for Rechargeable Magnesium Batteries, *Cell Rep. Phys. Sci.*, 2020, **1**, 100265.

106 Y. Tian, Y. An, C. Wei, H. Jiang, S. Xiong, J. Feng and Y. Qian, Recently advances and perspectives of anode-free rechargeable batteries, *Nano Energy*, 2020, **78**, 105344.

107 T. Wang, J. Sun, Y. Hua, B. N. V. Krishna, Q. Xi, W. Ai and J. S. Yu, Planar and dendrite-free zinc deposition enabled by exposed crystal plane optimization of zinc anode, *Energy Storage Mater.*, 2022, **53**, 273–304.

108 W. Yao, P. Zou, M. Wang, H. Zhan, F. Kang and C. Yang, Design Principle, Optimization Strategies, and Future Perspectives of Anode-Free Configurations for High-Energy Rechargeable Metal Batteries, *Electrochem. Energy Rev.*, 2021, **4**, 601–631.

109 K. Xu, X. Zheng, R. Luo, J. Sun, Y. Ma, N. Chen, M. Wang, L. Song, Q. Zhao and W. Chen, A three-dimensional zincophilic nano-copper host enables dendrite-free and anode-free Zn batteries, *Mater. Today Energy*, 2023, **34**, 101284.

110 X. Zheng, Z. Liu, J. Sun, R. Luo, K. Xu, M. Si, J. Kang, Y. Yuan, S. Liu, T. Ahmad, T. Jiang, N. Chen, M. Wang, Y. Xu, M. Chuai, Z. Zhu, Q. Peng, Y. Meng, K. Zhang, W. Wang and W. Chen, Constructing robust heterostructured interface for anode-free zinc batteries with ultrahigh capacities, *Nat. Commun.*, 2023, **14**, 76.

111 C. Wang, D. Wang, D. Lv, H. Peng, X. Song, J. Yang and Y. Qian, Interface Engineering by Hydrophilic and Zincophilic Aluminum Hydroxide Fluoride for Anode-Free Zinc Metal Batteries at Low Temperature, *Adv. Energy Mater.*, 2023, **13**, 2204388.

112 C. Wang, D. Wang, D. Lv, H. Peng, X. Song, J. Yang and Y. Qian, Interface Engineering by Hydrophilic and Zincophilic Aluminum Hydroxide Fluoride for Anode-Free Zinc Metal Batteries at Low Temperature, *Adv. Energy Mater.*, 2023, **13**, 2204388.

113 J. Duan, L. Min, M. Wu, T. Yang, M. Chen and C. Wang, “Anode-free” Zn/LiFePO<sub>4</sub> aqueous batteries boosted by hybrid electrolyte, *J. Ind. Eng. Chem.*, 2022, **114**, 317–322.

114 R. Qin, Y. Wang, M. Zhang, Y. Wang, S. Ding, A. Song, H. Yi, L. Yang, Y. Song, Y. Cui, J. Liu, Z. Wang, S. Li, Q. Zhao and F. Pan, Tuning Zn<sup>2+</sup> coordination environment to suppress dendrite formation for high-performance Zn-ion batteries, *Nano Energy*, 2021, **80**, 105478.

115 Y. An, B. Xu, Y. Tian, H. Shen, Q. Man, X. Liu, Y. Yang and M. Li, Reversible Zn electrodeposition enabled by

interfacial chemistry manipulation for high-energy anode-free Zn batteries, *Mater. Today*, 2023, **70**, 93–103.

116 H. Chen, M. Chen, W. Zhou, X. Han, B. Liu, W. Zhang and J. Chen, Flexible Ti3C2Tx/Nanocellulose Hybrid Film as a Stable Zn-free Anode for Aqueous Hybrid Zn-Li Batteries, *ACS Appl. Mater. Interfaces*, 2022, **14**, 6876–6884.

117 M. Zhou, S. Guo, J. Li, X. Luo, Z. Liu, T. Zhang, X. Cao, M. Long, B. Lu, A. Pan, G. Fang, J. Zhou and S. Liang, Surface-Preferred Crystal Plane for a Stable and Reversible Zinc Anode, *Adv. Mater.*, 2021, **33**, e2100187.

118 Y. Yan, C. Shu, T. Zeng, X. Wen, S. Liu, D. Deng and Y. Zeng, Surface-Preferred Crystal Plane Growth Enabled by Underpotential Deposited Monolayer toward Dendrite-Free Zinc Anode, *ACS Nano*, 2022, **16**, 9150–9162.

119 G. Wang, M. Zhu, G. Chen, Z. Qu, B. Kohn, U. Scheler, X. Chu, Y. Fu, O. G. Schmidt and X. Feng, An Anode-Free Zn-Graphite Battery, *Adv. Mater.*, 2022, **34**, e2201957.

120 A. VahidMohammadi, J. Rosen and Y. Gogotsi, The world of two-dimensional carbides and nitrides (MXenes), *Science*, 2021, **372**, eabf1581.

121 Y. An, Y. Tian, K. Zhang, Y. Liu, C. Liu, S. Xiong, J. Feng and Y. Qian, Stable Aqueous Anode-Free Zinc Batteries Enabled by Interfacial Engineering, *Adv. Funct. Mater.*, 2021, **31**, 2101886.

122 F. Ming, Y. Zhu, G. Huang, A.-H. Emwas, H. Liang, Y. Cui and H. N. Alshareef, Co-Solvent Electrolyte Engineering for Stable Anode-Free Zinc Metal Batteries, *J. Am. Chem. Soc.*, 2022, **144**, 7160–7170.

123 W. Sun, F. Wang, B. Zhang, M. Zhang, V. Küpers, X. Ji, C. Theile, P. Bieker, K. Xu, C. Wang and M. Winter, A rechargeable zinc-air battery based on zinc peroxide chemistry, *Science*, 2021, **371**, 46–51.

124 Y. Zhang, L. Wang, Q. Li, B. Hu, J. Kang, Y. Meng, Z. Zhao and H. Lu, Iodine Promoted Ultralow Zn Nucleation Overpotential and Zn-Rich Cathode for Low-Cost, Fast-Production and High-Energy Density Anode-Free Zn-Iodine Batteries, *Nano-Micro Lett.*, 2022, **14**, 208.

125 Y. Zhu, Y. Cui and H. N. Alshareef, An Anode-Free Zn-MnO<sub>2</sub> Battery, *Nano Lett.*, 2021, **21**, 1446–1453.

126 Z. A. Zafar, S. Imtiaz, R. Razaq, S. Ji, T. Huang, Z. Zhang, Y. Huang and J. A. Anderson, Cathode materials for rechargeable aluminum batteries: current status and progress, *J. Mater. Chem. A*, 2017, **5**, 5646–5660.

127 Q. Zhao, J. Zheng, Y. Deng and L. Archer, Regulating the growth of aluminum electrodeposits: towards anode-free Al batteries, *J. Mater. Chem. A*, 2020, **8**, 23231–23238.

128 L. Wang, X. Song, Y. Hu, W. Yan, Z. Tie and Z. Jin, Initial-anode-free aluminum ion batteries: In-depth monitoring and mechanism studies, *Energy Storage Mater.*, 2022, **44**, 461–468.

129 Z. Tong, B. Bazri, S.-F. Hu and R.-S. Liu, Interfacial chemistry in anode-free batteries: challenges and strategies, *J. Mater. Chem. A*, 2021, **9**, 7396–7406.

130 X. Shen, T. Sun, L. Yang, A. Krasnoslobodtsev, R. Sabirianov, M. Sealy, W.-N. Mei, Z. Wu and L. Tan, Ultra-fast charging in aluminum-ion batteries: electric double layers on active anode, *Nat. Commun.*, 2021, **12**, 820.

131 Y. Meng, J. Wang, M. Wang, Q. Peng, Z. Xie, Z. Zhu, Z. Liu, W. Wang, K. Zhang, H. Liu, Y. Ma, Z. Li and W. Chen, Anode-Free Aluminum Electrode with Ultralong Cycle Life and High Coulombic Efficiency Exceeding 99.92% Enabled by a Lattice-Matching Layer, *Adv. Energy Mater.*, 2023, **13**, 2301322.

132 S. K. Das, S. Mahapatra and H. Lahan, Aluminium-ion batteries: developments and challenges, *J. Mater. Chem. A*, 2017, **5**, 6347–6367.

133 Y. Zhang, S. Liu, Y. Ji, J. Ma and H. Yu, Emerging Nonaqueous Aluminum-Ion Batteries: Challenges, Status, and Perspectives, *Adv. Mater.*, 2018, **30**, e1706310.

134 C. Fang, B. Lu, G. Pawar, M. Zhang, D. Cheng, S. Chen, M. Ceja, J.-M. Doux, H. Musrock and M. Cai, Pressure-tailored lithium deposition and dissolution in lithium metal batteries, *Nat. Energy*, 2021, **6**, 987–994.